UC San Diego
UC San Diego Electronic Theses and Dissertations

Title

Endoplasmic Reticulum Stress in Mouse Models of Neurodegeneration

Permalink

https://escholarship.org/uc/item/50737722

Author

Chan, Priscilla

Publication Date

2016

Peer reviewed|Thesis/dissertation

UNIVERSITY OF CALIFORNIA, SAN DIEGO

Endoplasmic Reticulum Stress in Mouse Models of Neurodegeneration

A Thesis submitted in partial satisfaction for the requirements
for the degree of Master of Science

in

Biology

by

Priscilla Chan

Committee in Charge:

>Professor Jonathan H. Lin, Chair
>Professor Maho Niwa, Co-Chair
>Professor Randy Hampton

2016

The Thesis of Priscilla Chan is approved and it is acceptable in quality and form for publication on microfilm and electronically:

_____

_____

Co-Chair

_____

Chair

University of California, San Diego

2016

DEDICATION

This thesis is dedicated to my family,

Vincent, Sandy, and Dominic Chan,

for their endless support and love.

This thesis is also dedicated to my friends

who have been there to support me

since the beginning of my college career.

TABLE OF CONTENTS

LIST OF FIGURES AND TABLES

Chapter 1:

Chapter 2:

Chapter 3:

Chapter 4:

LIST OF ABBREVIATIONS

ONL	Outer nuclear layer
ER	Endoplasmic reticulum
UPR	Unfolded Protein Response
ATF6	Activating Transcription Factor 6
IRE1	Inositol-Requiring Enzyme 1
PERK	Protein kinase RNA-like Endoplasmic Reticulum Kinase
ERAD	Endoplasmic Reticulum-Associated Degradation
Rho	Human or mouse rhodopsin gene/proteins
RP	Retinitis Pigmentosa
ADRP	Autosomal Dominant Retinitis Pigmentosa
1NM-PP1	4-amino-1-*tert*-butyl-3-(1′-naphthylmethyl)pyrazolo[3,4-*d*]pyrimidine
DMF	Dimethylformamide
MAPT	Microtubule-associated protein tau
PHF	Paired helical filaments
NFT	Neurofibrillary tangles
AD	Alzheimer's disease
PSP	Progressive supranuclear palsy
CBD	Corticobasal degeneration

PiD	Pick's disease
GWAS	Genome wide association study
SNP	Single nucleotide polymorphism
LOAD	Late onset Alzheimer's Disease
STX6	Syntaxin-6
EIF2AK3	Eukaryotic Translation Initiation Factor 2 Alpha Kinase 3
MOBP	Myelin-Associated Oligodendrocyte Basic Protein
eIF2α	Eukaryotic translation initiation factor 2 subunit alpha
ERAI	Endoplasmic Reticulum Stress-Activated Indicator
Prnp	Prion protein
GFP	Green fluorescent protein
ERG	Electroretinogram
OCT	Optical coherence tomography
RPE	Retinal pigment epithelium

ACKNOWLEDGMENTS

I would like to thank the members of my thesis committee chair Professor Lin for his counsel regarding my project and for his career advice. I would also like to thank the other members of my committee Professor Niwa and Professor Hampton for their advice on my project.

I would like to thank the members of the Lin Lab: Dr. Wei-Chieh (Jerry) Chiang, Dr. Heike Kroeger, Dr. Nobuhiko Hiramatsu, Allen Chen, Chenxi Song, and Amanda Nguyen for their endless support. They have given me the opportunity to discuss and challenge my knowledge about science and to offer me life and career advice. Dr. Chiang and Dr. Hiramatsu specifically founded my project ideas and provided inspiration for experimental design.

Additionally, I would like to thank Dr. Karen Chang with her help regarding the PS19 project following Dr. Hiramatsu's departure from the Lin lab. Lastly, I would like to thank Dr. Kevin Cao for his advice and support.

Chapter 2, in part, is a reprint of material that has been submitted for publication as it may appear in Proceedings of the National Academy of Sciences of the United States of America, 2016. Wei-Chieh Chiang, 2016. This thesis author was the secondary investigator and author of this paper.

ABSTRACT OF THESIS

Endoplasmic Reticulum Stress in Mouse Models of Neurodegeneration

by

Priscilla Chan

Master of Science in Biology

University of California, San Diego, 2016

Professor Jonathan H. Lin, Chair
Professor Maho Niwa, Co-Chair

The endoplasmic reticulum is an organelle that responsible for the folding and processing of newly synthesized proteins. When unfolded or misfolded proteins accumulate in the ER and disrupt proper function this leads to a phenomenon known as

ER stress. When this occurs, the UPR is activated in order to reduce ER load and restore the ER to its normal function. ATF6, IRE1, and PERK are the three pathways of theUPR. Here, I studied ER stress and the UPR in relation to retinitis pigmentosa, achromatopsia, and retinal degeneration in a tauopathy mouse model. I found that P23H rhodopsin, which is one of the most common mutated proteins involved with the development of retinitis pigmentosa, is highly ubiquitinated by several E3 ubiquitin ligases in order to be targeted for degradation. In addition, knocking out ATF6 seems to increase activation of IRE1 and preserve rhodopsin levels in the case of $Rho^{+/P23H}$ mice. In the achromatopsia study, Class 2 ATF6 mutants experience constitutive transcriptional activation and Class 3 ATF6 mutants are transcriptionally inactive, which can help explain causation of disease development. In the preliminary studies of the PS19 mouse model, I found that there is retinal degeneration and loss of visual function occurring in these mice compared to their wildtype littermates.

Chapter 1 Expression of E3 Ubiquitin Ligases in P23H Rhodopsin Associated Retinitis Pigmentosa

1.1 Introduction

The retina is responsible for sensing, processing, and sending visual information collected from the outside environment to the brain. Photoreceptors, which are housed in the outer nuclear layer (ONL), are specialized sensory neurons that detect light and activate retinal circuitry. There are two types of photoreceptors: rods and cones (Sung and Chuang, 2010). Rod photoreceptors have slender, rod-shaped, modified cilia, termed outer segments, and comprise the majority of photoreceptors in the retina. They are activated under low light conditions meaning they are responsible for vision under dim and nocturnal conditions. Cone photoreceptors have a conical outer segment and are present at much less quantities in the retina compared to rods in all other vertebrates besides humans. They are highly concentrated in the macula region of the retina, the point of highest visual acuity and special resolution in humans. These photoreceptors are activated under higher intensity light conditions and are responsible for diurnal and color vision. More specifically, color vision is possible due to different cone photoreceptors characterized by their different wavelength sensitivities account. When rods and/or cone photoreceptors are damaged and dysfunctional, it leads to the development of human blinding diseases.

Photoreceptors produce proteins that have the unique ability to transform light signals into electrical signals and to maintain their structural integrity and lamination in the retina. (Sung and Chuang, 2010). Photoreceptors may replace these proteins through a daily process that involves essentially the "shedding" of their outer segment tips to

remove damaged proteins and to allow nearby retinal pigment epithelial cells to recycle essential nutrients back into the photoreceptor cells (Sung and Chuang, 2010). This process requires large amounts of energy and, as a result, photoreceptors are metabolically characterized as the most active cells in the body (Sung and Chuang, 2010 and Wong-Riley, 2010).

Retinitis pigmentosa (RP) is a retinal degenerative disease that affects approximately 1.5 million people globally (Berson, 1993). This disease is characterized by loss of light sensitivity, night blindness, and loss of peripheral vision that progressively worsens to affect central vision. Degeneration of the rod photoreceptors begin first which eventually leads to the loss of cone photoreceptors (Berson, 1993). RP is an umbrella term for the autosomal dominant, autosomal recessive, and X-linked subtypes of the disease (Dryja and Li, 1995). Mutations that occur in the rhodopsin (RHO) gene are a common cause for the development of autosomal dominant retinitis pigmentosa (Dryja et al., 1990).

Rhodopsin (Rho) is a 348 amino acid, G-protein-coupled transmembrane receptor protein exclusively expressed by rods (Palczewski, 2006). When Rho is linked to 11-*cis*-retinal, Rho is able to respond to light and initiate the phototransduction cascade that will convert light signals into electrical signals in the retina (Palczewski, 2012). Rho is necessary for photoreceptor function and survival given that Rho knockout mice (*Rho$^{-/-}$*) experience retinal degeneration at very earlier on (Humphries et al., 1997). There have been numerous Rho mutations that have been found to be linked to retinitis pigmentosa and many of these mutants cause missense changes that lead the mutant protein to

misfold and accumulate in the ER (Chiang et al., 2012, Chiang et al., 2014, Illing et al., 2002, Kaushal and Khorana, 1994 and Sung et al., 1991).

P23H rhodopsin, which contains a single amino acid change from proline to histadine at the amino acid position 23, is the most common cause of heritable retinitis pigmentosa in North America given that it is responsible for 10% of Autosomal Dominant Retinitis Pigmentosa (ADRP) patients (Dryja et al., 1991 and Dryja and Li, 1995). This mutant rhodopsin is unable to fold properly leading to its aggregation and failure to traffic properly out of the ER in rod photoreceptor cells (Saliba et al., 2002). As a result, P23H rhodopsin causes endoplasmic reticulum (ER) stress and activates the Unfolded Protein Response (UPR) (Kroeger et al., 2014 and Lin et al., 2007).

The ER is an organelle responsible for the synthesis, folding, and assembly of membrane and secreted proteins, lipid and sterol metabolism, and free calcium storage (Alberts, 2008). When unfolded or misfolded proteins accumulate in the ER and disrupt proper function, however, this leads to a phenomenon known as ER stress (Hetz and Mollereau, 2014, Hiramatsu et al., 2015 and Wang and Kaufman, 2016). Under these conditions, a multitude of genes are expressed as ER-resident or ER-associated proteins with the aim of clearing misfolded proteins or improving the ER folding microenvironment. This occurs in a series of processes known as the UPR, which is mediated by three ER resident transmembrane proteins: ATF6, IRE1, and PERK (Walter and Ron, 2011 and Wang and Kaufman, 2016). When these pathways are activated via ER stress, they initiate intracellular signal transduction pathways that will upregulate transcriptional proteins that enhance ER function by increasing ER size, ER protein folding enzymes and chaperones, and degradation of damaged proteins through the ER-

Associated Degradation (ERAD) system. In addition, PERK signaling also aims to reduce protein production by attenuating ribosome assembly on mRNAs. If these series of events are unable to alleviate ER stress, the IRE1 and PERK branches of the UPR will instead promote the expression of genes responsible for apoptosis (Tabas and Ron, 2011).

ER stress and UPR signaling are mechanisms that have been found in a wide variety of retinal degenerative as well as neurodegenerative diseases. In the case of RP and P23H rhodopsin, ER stress and UPR signaling occur in transgenic models of RP before they experience cell death (Kroeger et al., 2014 and Lin et al., 2007). This transgenic model closely mimicked the spatial distribution and temporal progression of photoreceptor cell death and vision loss that patients with the same mutation experienced (Sakami et al., 2011). Furthermore, it was found that the IRE1 branch of the UPR was activated in this mouse model given that the levels of XBP-1s mRNA, XBP-1 protein, and transcriptional targets were significantly increased in the retinas of $Rho^{P23H/P23H}$ mice (Chiang et al., 2015).

Many of XBP1's target genes encode for components of the ERAD pathway and these genes have been found to be upregulated in the retinas of $Rho^{+/P23H}$ mice (Chiang et al., 2015, Lee et al., 2003 and Shoulders et al., 2013). Under the ubiquitin-proteasome system of ERAD, ubiquitin, a small 76-amino acid protein, is covalently bonded to misfolded proteins by the sequential action of E1 activating, E2 conjugating, and E3 ligase enzymes and, from there, the ubiquitin-tagged proteins are recognized and degraded by the proteasome (Pickart, 2001).

As previously discovered by our lab, rhodopsin from $Rho^{P23H/P23H}$ mice was heavily ubiquitinated when immunoprecipitated from photoreceptors of $Rho^{+/P23H}$ mice

while the rhodopsin protein levels remained low in *Rho$^{P23H/P23H}$* mice despite comparable rhodopsin mRNA levels in both *Rho$^{P23H/P23H}$* and *Rho$^{+/+}$* (Chiang et al., 2015). These results show that the Rho^{P23H} protein is targeted for degradation via the ERAD pathway (Chiang et al., 2015). In addition, our lab also previously discovered, through mass spectrometry experiments, a number of E3 ubiquitin ligases that are associated with Rho^{P23H} (Chiang et al., 2015) (Table 1). Given that these mutant rhodopsin proteins have been found to be highly ubiquitylated prior to degradation, it is important to determine: 1. Which of these E3 ubiquitin ligases are most important for the ubiquitylation of Rho^{P23H} proteins? 2. How does the loss of these ligases affect the degradation of Rho^{P23H} protein? 3. Will the loss of these proteins promote retinal degeneration due to an accumulation of mutant Rho^{P23H} protein?

1.2 Results

Thirteen of the eighteen E3 ubiquitin ligases of were overexpressed in P23H rhodopsin mouse retinas

ERAD-related proteins were co-immunoprecipitated with P23H rhodopsin and through mass spectrometry, our collaborators were able to identify eighteen different E3 ubiquitin ligases that appear to be specifically associated with P23H rhodopsin but not with wildtype rhodopsin (Table 1) (Chiang et al., 2015). In order to determine whether these E3 ubiquitin ligases are actually expressed under P23H rhodopsin settings, we collected retinas of P30 mice that were either wildtype or $Rho^{P23H/P23H}$. Through RT-PCR experiments, I determined that all eighteen ubiquitin ligases were expressed in both wildtype and $Rho^{P23H/P23H}$ mice retinas (Figure 1). However, I noticed that some of the bands appeared to be stronger for some genes under the $Rho^{P23H/P23H}$ background and, consequently, decided to investigate this further by performing qPCR experiments to quantify the expression level of these genes.

Through the qPCR experiments, I found that out of the eighteen E3 ubiquitin ligases of interest, thirteen of the genes were expressed on average three times more in $Rho^{P23H/P23H}$ mice retinas compared to their wildtype counterpart (Figure 2). XBP-1s and ERdj4 were also expressed at higher levels in the $Rho^{P23H/P23H}$ retinas, suggesting that the IRE1 branch of the UPR is active and promoting the activation of ERAD (Chiang et al., 2015).

E3 ubiquitin ligases associated with P23H Rhodopsin are expressed in HEK293 cells

In order to confirm that these same E3 ubiquitin ligases can be expressed in human cells, I ran RT-PCR experiments on HEK 293 cells. Prior to lysis, the cell

were treated with 1NM-PPI in order to artificially activate the IRE1 or DMF as a control. IRE1 was activated in order to mirror the IRE1 activation seen in $Rho^{P23H/P23H}$ mice retinas. 1NM-PP1 binds selectively to the kinase domain of IRE1 mutants that have an enlarged ATP-binding site, therefore activating it (Papa et al., 2003). This particular cell line has a single amino acid change from isoleucine to glycine at the amino acid position 642 in the IRE1 protein, which leads the cells to be sensitive to 1NM-PP1. However, because conventional transfection or transduction gene activation leads to cell death because the UPR is constitutively active, a flippase-mediated, site-specific DNA recombination method was used to introduce the 1NM-PP1-sensitized IRE1 (I642G) mutant allele directly into the genome of HEK293 cells that bear a defined *frt* site (Tirasophon et al., 2000, Wang et al., 1998 and Cohen and Panning, 2007).

The RT-PCR experiments confirmed that all of the ubiquitin ligases of interest were expressed in both the control DMF and 1NM-PP1 treated cells (Figure 3). However, it is unclear whether the genes were expressed more under the 1NM-PP1 treated conditions.

1.3 Discussion

My preliminary studies highlight the potential role a number of E3 ubiquitin ligases have in the degradation process of P23H rhodopsin. Thirteen of the eighteen genes examined were expressed on average three times more under Rho$^{P23H/P23H}$ conditions in comparison to *Rho*$^{+/+}$. We know from previous studies that P23H rhodopsin is highly ubiquitinated and, consequently, subjected to degradation through the ubiquitin-proteasome system (Chiang et al., 2015 and Pickart, 2001). The next steps for this project would be to further investigate exactly which of these genes are necessary for the ubiquitination of mutant P23H rhodopsin. Also it will be important to determine whether the presence one of these ubiquitin ligases is sufficient to target P23H rhodopsin for degradation or will it be necessary to have more than one ubiquitin ligases adding ubiquitin tags onto these mutant proteins.

Given that so many of the genes observed were expressed at such high levels in *Rho*$^{P23H/P23H}$ mouse retinas, it is also important to determine whether the same results are observed in humans. In order to do so it will be necessary to run qPCR experiments on HEK293 treated with 1NM-PP1 to see if activating IRE1 under these conditions can upregulate the same E3 ubiquitin ligases, if not more of them, given that the IRE1 pathway is activated in response to P23H rhodopsin (Chiang et al., 2015).

1.4 Materials and Methods

Cell Culture

HEK293 cells were maintained at 37°C, 5% CO_2 in Dulbecco's modified Eagle medium (Mediatech, Manassas, VA) supplemented with 10% fetal calf serum (Mediatech), and 1% penicillin/streptomycin (Invitrogen, Carlsbad, CA).

Animals

Homozygous breeding pairs of P23H rod opsin knock-in mice were maintained to produce $Rho^{P23H/P23H}$ homozygotes. C57BL/6J mice were used as wild-type controls ($Rho^{+/+}$). Mice were maintained in a barrier animal facility in a 12:12 light cycle at in-cage irradiance of less than 125 lux and provided standard mouse chow (UCSD). Retinal tissues were collected from the animals of either sex for 12 days of age. The UCSD Animal Care staff checked mice daily. In addition, laboratory personnel checked births in the morning and evening during the light phase of the light cycle to determine exact birthdates because early eye developmental and degenerative events occurred rapidly once they commenced. All animal studies followed the guidelines of the institutional animal care committees at UCSD and were conducted in accordance with the recommendations of the American Veterinary Medical Association Panel on Euthanasia and the Association of Research for Vision and Ophthalmology.

Molecular Biology

Retinas and cells were lysed and total RNA was collected with a RNeasy mini kit (Qiagen, Germany). mRNA was reverse-transcribed with the iScript cDNA Synthesis Kit (Bio-Rad, Hercules, CA).

For real time PCR and quantitative PCR analyses, cDNA was used as template in 2

x M-PCR OPTI Mix (Biotool) and SYBR green qPCR supermix (Bio-Rad). Primers used include: mouse *Rpl19*: 5′-ATGCCAACTCCCGTCAGCAG- 3′ and 5′-TCATCCTTCTCATCCAGGTCACC-3′; mouse *Nedd4*, 5'-CACCAGAACCCTCTCCCCTA and 5'- TTGTCAGGGCCATCCACATC-3'; mouse *Trim21*, 5'- TCCCATGGTGGAGCCTATGA-3' and 5'-CAGTGCGTTTCCTGGGTACT-3'; mouse *Kcmf11*, 5'-CCTCCACAACTCCCAGTTCC-3' and 5'- ACACAGCCCATAGCACCAAA-3'; mouse *Syn1*, 5'- ACACACTACTGGATGCTGCC-3' and 5'-GCTTCAGGAATTGGTGGGGA-3'; mouse *Huwe1*, 5'-CTCTCGTGGGGACTCTGGTA-3' and 5'- TTTGGTGGTCTGTGGTTGCT-3'; mouse *Mycbp2*, 5'- GGTCGGAGGTTGATGGACTT-3' and 5'-TCATACTCATGGATGCCGCC-3'; mouse *Hecw1*, 5'-ACCATGGCAACAGAGAGAGC-3' and 5'- TGAACTTGACCGCTGGAGAC-3'; mouse *Amfr*, 5'- AAGGAAACTGCCCTGTGGACATC-3' and 5'-GATTGTGCTGGTTCAAGCGAGG-3'; mouse *Ubr4*, 5'-CAACAACCGAACTGTGCAGG-3' and 5'- ACTGCAGCGAGGACATTGAA-3'; mouse *Ubr5*, 5'- TGAAGCCATACCCTTGGCTG-3' and 5'-CTGCCGGTTTTGCATGTTCA-3'; mouse *Rnf170*, 5'-CATACTGGCGATACGGGTCC-3' and 5'- AACGCATGTCTCAGCAAGGT-3'; mouse *Rnf213*, 5'- GCTTCCCAGAAGGCTCCATT-3' and 5'-GTGGCCAACTTGCCTTTGAG-3'; mouse *March5*, 5'-TGTGGAGCCCTTGTCTTTCC-3' and 5'- TAGGATTTTGCGGTGTGCCT-3'; mouse *Hectd1*, 5'- GAAGAACGCCAGTGGACAGA-3' and 5'-

TAACACGTGCTCCTGGAACC-3'; mouse *Trim41*, 5'-

CTTGCTTGCTGAAGCCCAAG-3' and 5'- TGCAGCCTGACAAAACATGC-3';

mouse *Herc2*, 5'- CAGTGCCAGCACTTTGACAC-3' and 5'-

TCCAGCTGCTCAAACGTCAT-3'; mouse *Trim36*, 5'-

TGCCAAGGGCAAGGTGACTA-3' and 5'- TTTGAGCTGTCTGACGCCAC-3';

mouse *Zswim2*, 5'- CCAGTGTCGACTTTGCTTGA-3' and 5'-

TGATGTGCTTGTCCATCCGT-3', human *RPL19*, 5'-

ATGTATCACAGCCTGTACCTG-3' and 5'-TTCTTGGTCTCTTCCTCCTTG-3';

human *Nedd4*, 5'- AGTTCTGCAGGCCCTCAATC and 5'-

TCCTCTCAGATGGGCTGGAA -3'; human *Trim21*, 5'-

GAGAAGCTCCAGGTGGCATT-3' and 5'- TCTCAGCTGCTCCCTCTCAT-3'; human

Kcmf11, 5'- AGGTCCTCGTGCTCGTAGAT-3' and 5'-

TAACTGAGAAGCGGAAGGGC-3'; human *Syn1*, 5'-

CCACTGTGGTGTACCTGACC-3' and 5'- GGGCTGAAGTCATCCCGAAA-3';

human *Huwe1*, 5'- ATGCCTGACAGCTACCCAAC-3' and 5'-

GTGGGACCCAATTCCTCTGG-3'; human *Mycbp2*, 5'-

AGCTAGAGACAGAGGCGGAA-3' and 5'- GTTTCCTCGATCACCTTTGCT-3';

human *Hecw1*, 5'- CCCGAGTTCTTCACTGTGCT-3' and 5'-

TCCGTTTTGATCTCCCAGCC-3'; human *Amfr*, 5'- ACCTGATGGTTCAGCTCTGC-

3' and 5'- CCATGAAAGCCAAGGTGTGC-3'; human *Ubr4*, 5'-

CGGGAACACCCTGACGTAAA-3' and 5'- GCTCCTCGATCAGCTCTTCC-3';

human *Ubr5*, 5'- AGAGCCTCCAAGATTTGCCC-3' and 5'-

GAGTGAAACAGTCCAGCCGA-3'; human *Rnf170*, 5'-

TCACCCAGAAAACCAGGAGC-3' and 5'- GATTGCCCCAAGCCATGAAC-3';

human *Rnf213*, 5'- CTTCACCCAGTTCGAGCAGT-3' and 5'-

CCACAGGCAAAAAGTCCGTG-3'; human *March5*, 5'-

CGAATCTTGTGTGGAGCCCT-3' and 5'- AATTTTGCGGTGTGCCTGTC-3'; human

Hectd1, 5'- TTAGGCGAGATGACCCTGGA-3' and 5'-

TGCTGCCACCAGAGCATAAA-3'; human *Trim41*, 5'-

ACCAAGAAGCCCTGAAGCTC-3' and 5'- CATCTTCTGCACTGCCTCCA-3';

human *Herc2*, 5'- GGGGCCCAGTTAGAGGACTA-3' and 5'-

AACTGCACGGTGATTTTGCC-3'; human *Trim36*, 5'-

TCGGAGTCTGGGGAGATGAG-3' and 5'- TTGCATGCTGGGCAAATGAG-3'; and

human *Zswim2*, 5'- AAGACACTTGAGCGAGAGGC-3' and 5'-

CAAAGTTCCCCTCCTTTCGGA-3'.

*Rpl1*9 mRNA levels served as internal normalization standards. RT-PCR and qPCR

conditions were 95°C for 5 min; 95°C for 10 sec; 60°C for 10 sec; 72°C for 10 sec, with

40 cycles of amplification

1.5 Figures and Table

Table 1. E3 Ubiquitin Ligases Associated with P23H Rhodopsin
Eighteen different E3 ubiquitin ligases were found to be associated with mutant P23H rhodopsin protein in Rho$^{P23H/P23H}$ mice retinas through mass spectrometry experiments.

Name	Abbrev.	A.A.	Mass (kDa)
E3 ubiquitin-protein ligase neural precursor cell expressed developmentally down-regulated protein 4	Nedd4	887	102.7
E3 ubiquitin-protein ligase tripartite motif-containing protein 21	Trim21	470	54.2
Isoform 2 of E3 ubiquitin-protein ligase potassium channel modulatory factor 1	Kcmf1	381	41.8
E3 ubiquitin-protein ligase synoviolin 1	Syvn1	612	67.3
Isoform 3 of E3 ubiquitin-protein ligase HECT, UBA, and WWE Domain Containing 1	Huwe1	4377	482.6
Isoform 2 of Probable E3 ubiquitin-protein ligase myc-binding protein 2	Mycbp2	4711	517.7
Isoform 2 of E3 ubiquitin-protein ligase HECT, C2, and WW domain containing 1	Hecw1	1604	179.5
E3 ubiquitin-protein ligase autocrine motility factor receptor	Amfr	643	73.1
Isoform 3 of E3 ubiquitin-protein ligase 600 kDa retinoblastoma protein-associated factor	Ubr4	5180	572.3
Isoform 3 of E3 ubiquitin-protein ligase HECT domain-containing 1	Ubr5	2792	308.4
E3 ubiquitin-protein ligase RING finger protein 170	Rnf170	286	33.4
E3 ubiquitin-protein ligase RING finger protein 213	Rnf213	5150	584.5
E3 ubiquitin-protein ligase membrane-associated RING finger protein 5	March5	278	31.2
E3 ubiquitin-protein ligase HECT domain-containing protein 1	Hectd1	2618	290.1
E3 ubiquitin-protein ligase tripartite motif-containing protein 41	Trim41	630	71.8
E3 ubiquitin-protein ligase HECT domain and RCC1-like domain-containing protein 2	Herc2	4836	527.5
E3 ubiquitin-protein ligase tripartite motif-containing protein 36	Trim36	729	82.8
E3 ubiquitin-protein ligase zinc finger SWIM domain-containing protein 2	Zswim2	631	71.8
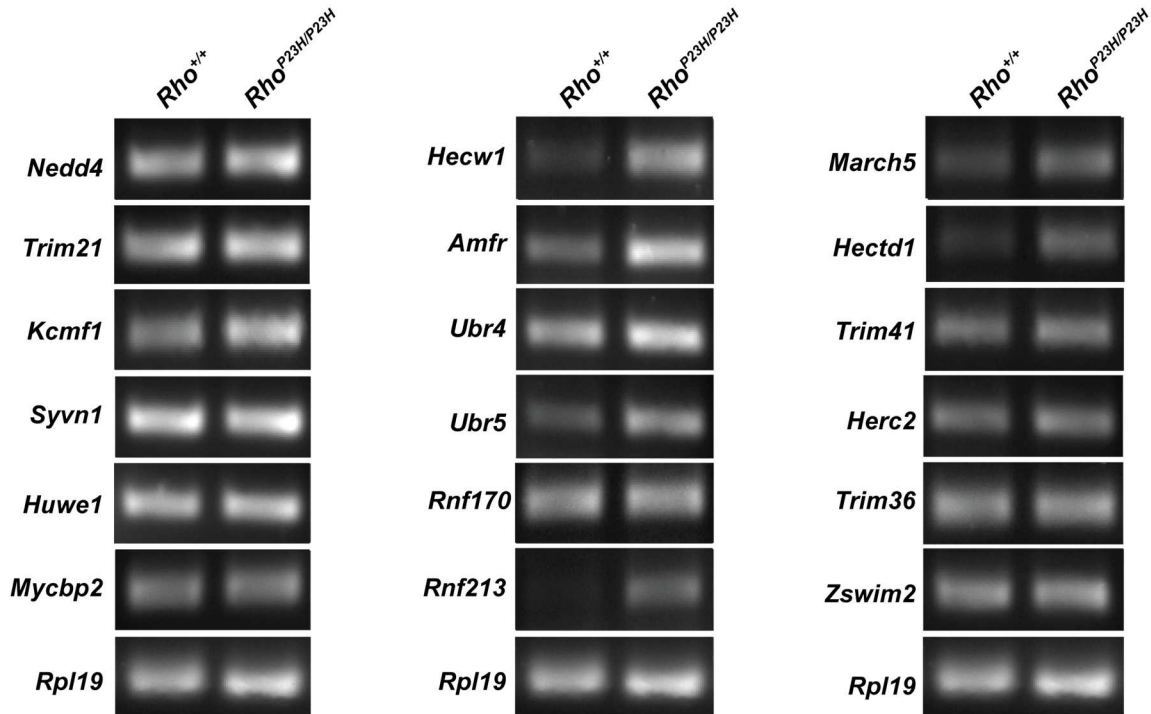
Figure 1. E3 ubiquitin ligases of interest are all expressed in $Rho^{+/+}$ and $Rho^{P23H/P23H}$ mouse retinas

Retina samples were extracted from post-natal day (P) 30 mice that were either $Rho^{+/+}$ or $Rho^{P23H/P23H}$ genotypes. RT-PCR experiments were performed to determine the expression of all eighteen ubiquitin ligases in the mice retinas. The left lanes contain PCR products from the $Rho^{+/+}$ mice, and the right lanes contain PCR products from the $Rho^{P23H/P23H}$ mice.
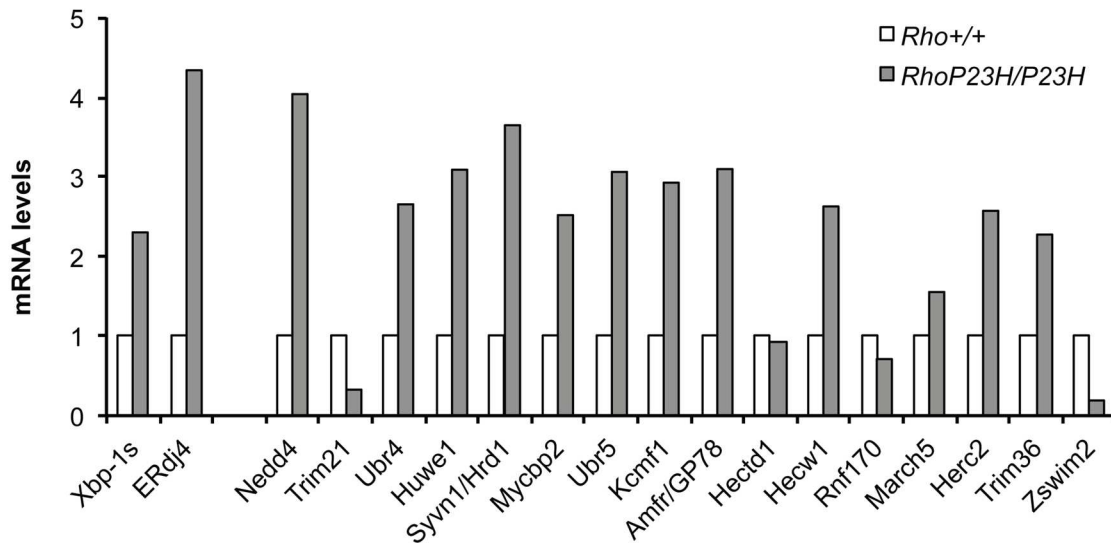
Figure 2. Thirteen of the eighteen E3 ubiquitin ligases are expressed more in $Rho^{P23H/P23H}$ mouse retinas

Mouse retinas were collected to isolate cDNA in order to examine mRNA levels of the genes of interest. The expression levels for all the E3 ubiquitin ligases were measured through real-time quantitative PCR. Only the *Trim21, Hectd1, Rnf170,* and *Zswim2* genes did not appear to be upregulated due to the presence of mutant P23H rhodopsin. XBP-1s and ERdj4 mRNA levels were measured to confirm the activation of IRE1 in the $Rho^{P23H/P23H}$ mouse retinas.
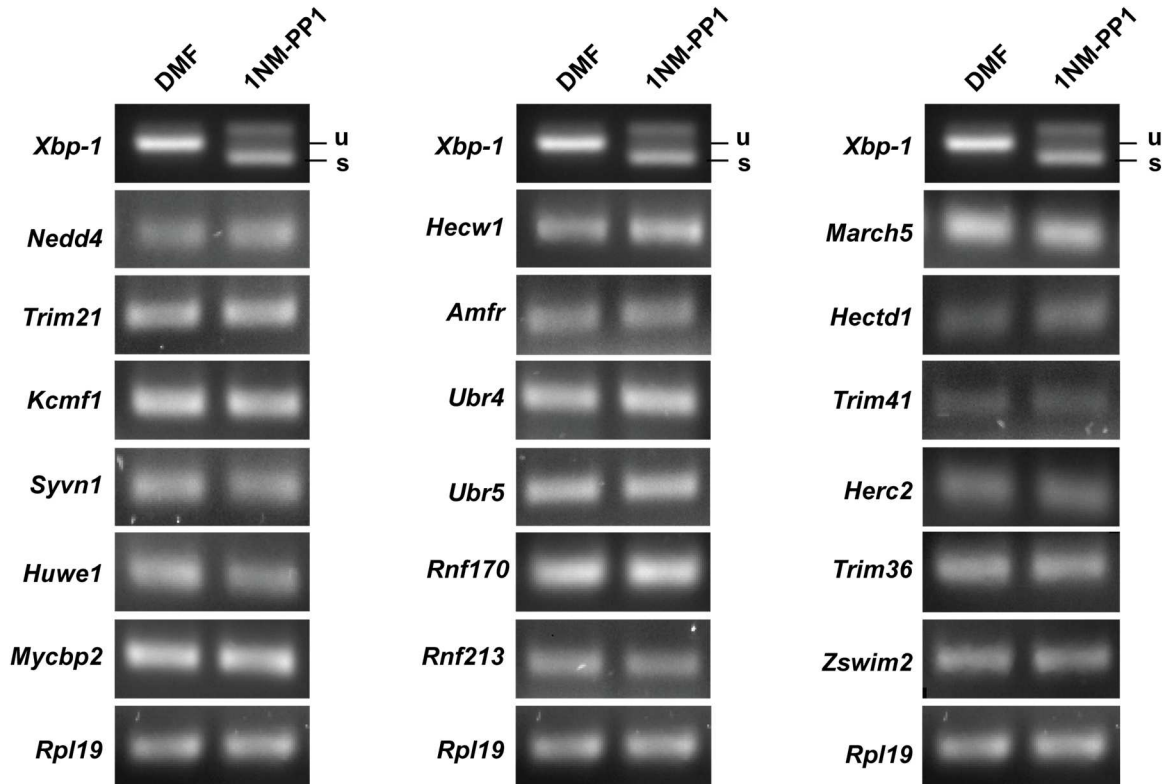
Figure 3. E3 ubiquitin ligases of interest are expressed in HEK293 cells under both IRE1 inactive and active conditions

HEK293 cells were treated with 1NM-PP1 to artificially activate the IRE1 pathway, with DMF as a negative control. RNA samples were collected from these cells to generate cDNA, which was then used to perform RT-PCR experiments. The left lanes contain PCR products from the DMF-only treated cells and the right lanes contain PCR products from the 1NM-PP1 treated cells.

Chapter 2 Functional Diversity of Human ATF6 Mutations Associated with

Achromatopsia

2.1 Introduction

Achromatopsia is an autosomal recessive retinal degenerative disease that affects 1 in 33,000 people throughout the country. This disease is characterized by dysfunction and degeneration of cone photoreceptors, which are responsible for color vision. Patients with incomplete achromatopsia may still retain some color vision but patients with complete achromatopsia can only see black, white, and shades of gray. Patients also experience photophobia, nystagmus, and significantly impaired visual acuity. Symptoms are usually presented at birth or within the first few months of life. Mutations in cone phototranduction genes, GNAT2, PDE6C, PDE6H, CNGA3, and CNGB3 are found in ~80-90% of achromatopsia patients (Chang et al., 2009, Kohl et al., 1998, Kohl et al., 2000, Kohl et al., 2012 and Thiadens et al., 2009). More recently, however, it was discovered that the *ATF6* gene was mutated in some patients with achromatopsia but had normal cone phototransduction genes (Ansar et al., 2015, Kohl et al., 2015 and Xu et al., 2015).

The ATF6 protein is one of three different ER-resident transmembrane proteins that regulate the UPR (Haze et al., 1999 and Walter and Ron, 2011). Under ER stress conditions, the full length ~90 kDa protein translocates from the ER to the Golgi apparatus where site 1 and site 2 proteases cleave the protein, resulting in the liberation of the ~50 kDa cytoplasmic portion of the ATF6 (Ye et al., 2000). The cytosolic portion of the ATF6 protein contains a bZIP transcriptional activator. The cytosolic portion of ATF6 will then migrate from the Golgi to the nucleus to activate its target genes, such as

17

ER protein folding enzymes and chaperones, in order to maintain ER and cellular homeostasis (Haze et al., 1999, Wu et al., 2007 and Yamamoto et al., 2007).

The *ATF6* mutations discovered in achromatopsia patients, who are either homozygous or compound heterozygous for the mutations, are found throughout the entire gene and include missense, nonsense, splice site, and frame shift mutations (Ansar et al., 2015, Kohl et al., 2015 and Xu et al., 2015). Fibroblasts were collected from achromatopsia patients revealed compromised ATF6 signaling that varied by mechanism based on the location of the mutation on the *ATF6* gene. *ATF6* mutations that occurring in the luminal domain, known as Class 1 *ATF6* mutations, led to the impairment of trafficking the full length ATF6 protein from the ER to the Golgi when the UPR is activated. *ATF6* mutations that are located in the cytosolic domain and led to a truncated or damaged bZIP/transcriptional activator, known as Class 3 *ATF6* mutations, inhibited transcriptional activation of ATF6 target genes. Also, further analysis performed on *ATF*$^{-/-}$ mice revealed that they experienced photoreceptor dysfunction and cell death but this was only seen in mice that were of much older age (Kohl et al., 2015). These findings highlight ATF6 as a cause of achromatopsia, in addition to various phototransduction genes, and suggest that ER stress is an important pathogenic mechanism involved with cone dysfunction and consequent degeneration. Given these novel findings, it is important to address 1. How does ATF6 play a role in cone function and survival? How does the loss of ATF6 lead to the loss of photoreceptor function? How do other *ATF6* mutations found in achromatopsia patients cause ATF6 dysfunction, therefore leading to disease development?

2.2 Results

Class 2 ATF6 mutants experience constitutive transcriptional activation

Three of the *ATF6* mutations found in achromatopsia patients were predicted to produce ATF6 fragments of similar size to the full length ATF6 transcriptionally active fragment (Kohl et al., 2015 and Xu et al., 2015). The amino terminal domain of ATF6 is a 370-380 amino acid large transcriptional factor of the basic-leucine zipper family. ATF6 fragments that contain only the first 373 amino acids from the ATF6's cytosolic domain retains the transcriptional activity of ATF6 in mammalian cells (Haze et al., 1999 and Chiang et al., 2015). In order to test our predictions, I expressed a recombinant FLAG-tagged ATF6 containing a mutation that led to a single amino acid switch from valine to serine at the amino acid residue 371 of ATF6 followed by a stop codon three amino acids distally, ATF6[V371Sfs*3] into HEK293 cells via transfection. The mutant ATF6 protein showed almost the same size mobility as full length ATF6(373) transfected into the same cell line (Figure 4A). In addition to this, we also found that the V371Sfs*3 mutant transcriptionally upregulated ATF6 downstream target genes, *GrP78/BiP, HerpUD1, and Sel1, and Chop*, at levels as high as the full length ATF6 protein (Figure 4B). These results suggest that the mutant ATF6 protein produces a filly functional transcriptional activator under *in vitro* conditions. However, given that the nonsense and premature stop codons found in this mutant construct, the amount of functional truncated V371Sfs*3 ATF6 mutant protein may significantly less than the amount of wildtype ATF6 protein produced because the mutant mRNA transcripts may be subjected to nonsense-mediated mRNA decay (Kohl et al., 2015).

Class 3 ATF6 mutants are transcriptionally inactive

Five of the identified *ATF6* mutations in achromatopsia patients introduce nonsense or premature codons in exons encoding for the cytosolic domain of ATF6. Given the location of such mutations, it is predicted that the resulting ATF6 cytosolic protein fragment contains a non-functional bZIP or lacks the entire bZIP and transcriptional activator domain (Kohl et al., 2015 and Ansar et al., 2015). As done in the Class 2 mutant studies, I expressed two different recombinant FLAG-tagged ATF6 constructs containing a Class 3 ATF6 mutation into HEK293 cells. The ATF6[P118Lfs*31] mutant contains a proline to leucine amino acid change at the amino acid residue 118 followed by a premature stop codon 31 amino acids distally. This mutant ATF6 protein lacks the bZIP domain and part of the transcriptional activator domain. The other mutant, ATF6[N267*], contains a stop codon at the amino acid residue 267 and lacks only the bZIP domain. We were able to detect protein expression of the truncated ATF6 mutants in these transfected cells but there was no transcriptional induction of ATF6 downstream targets (Figures 4A and B). These results suggest that the disruption of transcriptional activity due to the truncation of the bZIP and/or transcriptional activator domain in these mutants results in the loss of ATF6 downstream function.

2.3 Discussion

The studies lay the groundwork the functional and mechanistic classification of the *ATF6* mutations that were identified in achromatopsia patients (Kohl et al., 2015). By studying the ATF6[V371Sfs*3] mutant, we found that Class 2 mutants present itself near the transmembrane domain of ATF6 and is able to produce the entire cytosolic ATF6 fragment that has fully functional ATF6 transcriptional activity (Figure 4B). However, given that all of the Class 2 mutants have premature stop codons it is likely that the resulting proteins are targets of nonsense mediated mRNA decay (Kohl et al., 2015). Such mechanisms can reduce mRNA transcript levels by 50-85% (Zetoune et al., 2008).

In the case of the Class 3 mutants studied, these mutations affected the cytosolic domain of ATF6 and therefore lacked or had defective bZIP/transcriptional activator domains. These cells expressing the ATF6[P118Lfs*31] or ATF6[N267*] mutations experienced the loss of ATF6 downstream function. The two Class 3 mutants studied were not able to transcriptionally or translationally activate downstream targets of ATF6 (Figure 4).

These studies highlight the diversity in molecular defects that arise due to the presence of these different classes of *ATF6* mutations and suggest that there are various ways mutations occurring in *ATF6* can lead to the development of achromatopsia. The results seen by purely expressing the mutants in HEK293 must be confirmed through analyses of patient fibroblast bearing the same mutations. Once we confirm the functional and mechanisms of the different *ATF6* mutations, it can be possible to begin exploring therapeutic strategies for patients that carry these mutations.

2.4 Materials and Methods

Cell Culture

HEK293 cells were maintained at 37°C, 5% CO_2 in Dulbecco's modified Eagle medium (Mediatech, Manassas, VA) supplemented with 10% fetal calf serum (Mediatech), and 1% penicillin/streptomycin (Invitrogen, Carlsbad, CA).

Plasmid construction and transfection

To generate ATF6[P118Lfs*31], ATF6[N267*], and ATF6[V371Sfs*3] expression plasmid, mutation was introduced into FLAG-tag-ATF6(373).pcDNA3.1 plasmid by site-direct mutagenesis using overlapping PCR. To express wild-type or mutant ATF6 in the cell culture system, plasmids containing the cDNA of those genes were transiently transfected to HEK293 using Lipofectamine 2000 (Invitrogen).

Molecular Biology

Cells were lysed and total RNA was collected using the RNeasy mini kit according to manufacturer's instructions (Qiagen, Hilden, Germany). mRNA was reverse-transcribed using the iScript cDNA Synthesis Kit (Bio-Rad, Hercules, CA).

For quantitative PCR analysis, cDNA was used as template in SYBR green qPCR supermix (Bio-Rad). Primers used include: human *RPL19*, 5'-ATGTATCACAGCCTGTACCTG-3' and 5'-TTCTTGGTCTCTTCCTCCTTG-3'; human *GRP78*, 5'-GCCTGTATTTCTAGACCTGCC-3' and 5'-TTCATCTTGCCAGCCAGTTG-3'; human *HerpUD1*, 5′-AACGGCATGTTTTGCATCTG-3′ and 5′-GGGGAAGAAAGGTTCCGAAG-3′; human *Sel1L*, 5′-ATCTCCAAAAGGCAGCAAGC-3′ and 5′-TGGGAGAGCCTTCCTCAGTC-3′; human *Chop*, 5′-ACCAAGGGAGAACCAGGAAACG-3′ and 5′-

TCACCATTCGGTCAATCAGAGC-3′;

Rpl19 mRNA levels served as internal normalization standards. qPCR condition was 95°C for 5 min; 95°C for 10 sec; 60°C for 10 sec; 72°C for 10 sec, with 40 cycles of amplification.

Immunoblotting Analysis

HEK293 cells expressing wildtype or mutant ATF6 were lysed in SDS lysis buffer (2% SDS, 62.5 mM Tris-HCl pH 6.8, containing protease inhibitors (Sigma-Aldrich), and phosphatase inhibitor (Thermo Scientific, Rockford, IL)). Protein concentrations of the total cell lysates were determined by BCA protein assay (Pierce, Rockford, IL). Equal amounts of protein were loaded onto 10% or 4-15% Mini-PROTEAN TGX precast gels (Bio-Rad) and analyzed by Western blot. The following antibodies and dilutions were used: anti-FLAG at 1:5000 (Sigma-Aldrich, St. Louis, MO); anti-GFP at 1:1000 (Santa Cruz Biotechnologies, Santa Cruz, CA); anti-human ATF6α antibody at 1:1000 (Abcam, Cambridge, MA); anti-BiP/GRP78 at 1:1000, anti-GAPDH at 1:5000, anti-HSP90 at 1:5000 (GeneTex Inc, Irvine, CA). After overnight incubation with primary antibody, membranes were washed in TBS with 0.1% Tween-20 (TBST) followed by incubation of a horseradish peroxidase-coupled secondary antibody (Cell signaling, Danvers, MA). Immunoreactivity was detected using the SuperSignal West chemiluminescent substrate (Pierce).

2.5 Figures

Figure 4. Transcriptional activator properties of Class 2 and Class 3 mutant *ATF6* proteins
(A) FLAG-tagged ATF6(373), ATF6[V371Sfs*3] (a Class 2 mutant), and ATF6[P118Lfs*31] and ATF6[N267*] (Class 3 mutants) were co-transfected with GFP into HEK293 cells. Immunoblotting was used to detect GRP78/BiP, GFP, and ATF6 protein using both anti-ATF6 and anti-FLAG antibodies. HSP90 protein levels were assessed as a loading control. (B) ATF6(373), ATF6[P118Lfs*31], ATF6[N267*], and ATF6[V371Sfs*3] were expressed in the HEK293 cells and mRNA was collected. Levels of genes transcriptionally regulated by ATF6, including *BiP/Grp78, HerpUD1, and Sel1l* were measured by real-time quantitative PCR and normalized to levels in mock transfected cells. *CHOP,* a gene that is regulated by PERK activation, was also assessed.

A
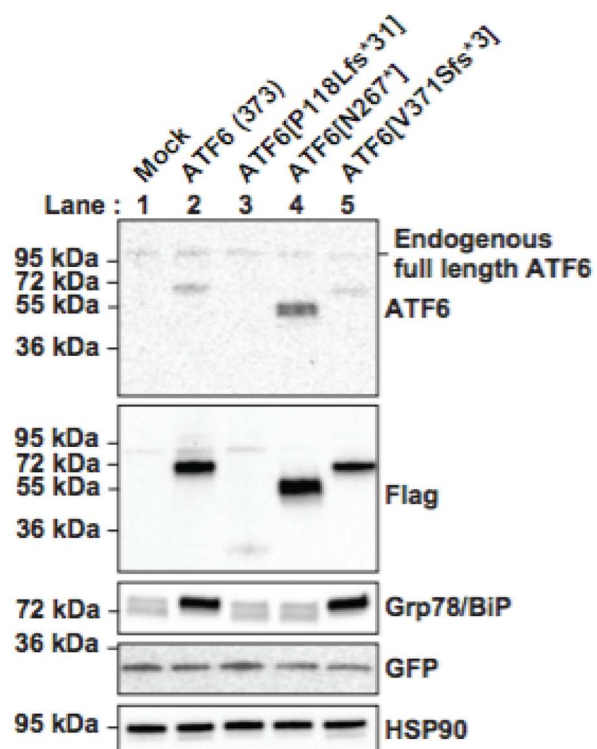
B
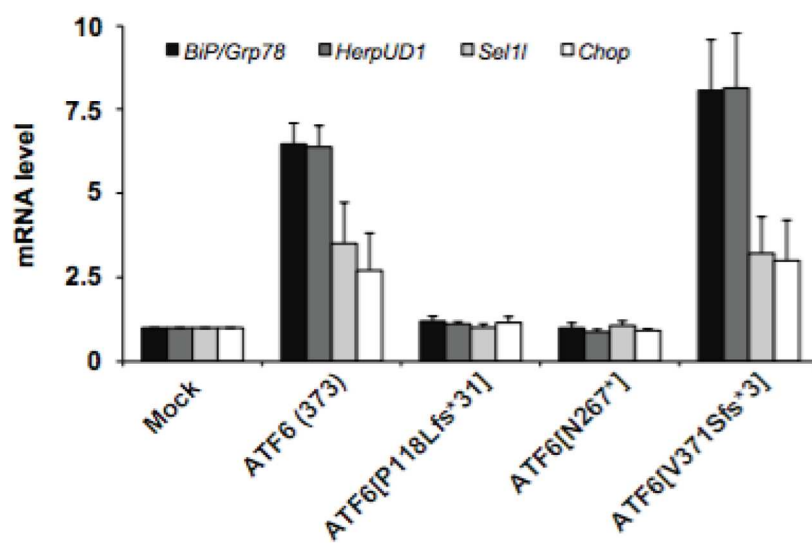
2.6 Manuscript Reprint

ABSTRACT

Achromatopsia is an autosomal recessive disorder characterized □by cone photoreceptor dysfunction. We recently identified *Activating Transcription Factor 6 (ATF6)* as a novel genetic cause of □achromatopsia. ATF6 is a key regulator of the Unfolded Protein □Response. In response to endoplasmic reticulum (ER) stress, ATF6 □migrates from the ER to Golgi to undergo regulated intramem- brane proteolysis to release a cytosolic domain containing a bZIP □transcriptional activator. The cleaved ATF6 fragment migrates to □the nucleus to transcriptionally upregulate protein folding enzymes and chaperones. *ATF6* mutations in achromatopsia patients include missense, nonsense, splice site, and single-nucleotide deletion or duplication changes found across the entire gene. Here, we □comprehensively tested the function of achromatopsia-associated □ATF6 mutations and found that they group into three distinct □molecular pathomechanisms. Class 1 ATF6 mutants show impaired ER to Golgi trafficking and diminished regulated intramembrane proteolysis and transcriptional activity. Class 2 ATF6 mutants bear □the entire ATF6 cytosolic domain with fully intact transcriptional activity and constitutive induction of downstream target genes □even in the absence of ER stress. Class 3 ATF6 mutants have complete loss of transcriptional activity due to absent or defective bZIP □domains. Primary fibroblasts from patients with Class 1 or Class 3 □ATF6 mutations show increased cell death in response to ER stress. □Our findings reveal that human ATF6 mutations interrupt distinct □sequential steps of the ATF6 activation mechanism. We

26

suggest ☐that increased susceptibility to ER stress-induced damage during ☐retinal development underlies the pathology of achromatopsia in ☐ patients with ATF6 mutations. ☐

INTRODUCTION

Achromatopsia is a heritable, blinding disease caused by cone photoreceptor dysfunction that spares the rod system. Using next-generation whole exome sequencing, we recently discovered autosomal recessive mutations in the *Activating Transcription Factor 6 (ATF6)* gene in patients with achromatopsia (Kohl et. al., 2015). *ATF6* mutations span the entire coding region and include missense, nonsense, splice site, and single nucleotide deletion and duplication changes (Kohl et al., Ansar et al., 2015, Xu et al., 2015). We previously showed that a missense mutation that introduced an arginine to cysteine substitution at residue 324 of the ATF6 protein compromised ATF6 activity in patient fibroblasts obtained from an achromatopsia family (Kohl et. al., 2015). However, the functional consequences of the other *ATF6* mutations found in achromatopsia patients remain unknown.

In people, ATF6 is a 670 amino acid glycosylated transmembrane protein found in the endoplasmic reticulum (ER) (Haze et al., 1999). In response to protein misfolding in the ER or other forms of ER stress, ATF6 migrates from the ER to the Golgi apparatus, where the S1P and S2P proteases cleave ATF6 in the transmembrane domain to liberate the cytosolic domain of ATF6 (Haze et al., 1999, Ye et al., 2000, Shen et al., 2002). The cytosolic domain of ATF6 contains a transcription factor of the basic leucine zipper (bZIP) family (Haze et al., 1999). Upon release from the Golgi membrane, the free

ATF6 cytosolic transcriptional activator fragment migrates to the nucleus to bind DNA and transcriptionally upregulate target genes that include ER protein folding chaperones and enzymes (Haze et al., 1999, Wu et al., 2007, Yamamoto et al., 2007). By this signal transduction mechanism, ATF6 activation helps restore ER protein folding homeostasis and alleviates ER stress (Nadanaka et al., 2004).

Here, we investigated how *ATF6* mutations found in achromatopsia patients affect ATF6's molecular mechanism of signaling and activation using patient fibroblasts, and recombinant mutant ATF6 proteins. We identified a class of *ATF6* mutations in the luminal domain that reduce ATF6 signaling by impairment of ER to Golgi trafficking of full-length ATF6 during ER stress. We identified a second class of *ATF6* mutations near the transmembrane domain that had the potential to produce intact ATF6 cytosolic fragment with fully functional transcriptional activator properties. Last, we identified a third class of *ATF6* mutations in the cytosolic domain that cause the loss of ATF6 function by deletion or mutation of the bZIP and/or transcriptional activator domain. Patient fibroblasts with loss-of-function *ATF6* mutations exhibited significantly increased cell death in response to ER stress.

RESULTS

The Class 1 ATF6[Y567N] mutation impairs ER-to-Golgi trafficking during ER stress

Four achromatopsia-associated ATF6 mutations introduce missense or frame shift changes in exons encoding the ER luminal domain of ATF6 (Kohl et al., 2015 and Xu et al., 2015). We previously identified a family with a tyrosine to asparagine substitution at position 567 in the luminal domain of ATF6(Kohl et al., 2015). We obtained fibroblasts

from two unaffected heterozygous ($ATF6^{Y567N/+}$) parents, probands #1 and #2, and a

homozygous ($ATF6^{Y567N/Y567N}$) affected child, patient #3 (Fig. 1A). We found equivalent

levels of $ATF6$ mRNA and full length ATF6 protein in heterozygous and homozygous

fibroblasts under standard cell culturing conditions (Fig. 1B, 1C). During experimentally

induced ER stress conditions by tunicamycin application, $ATF6$ mRNA levels and the

full-length ATF6 protein levels were upregulated in both heterozygous and homozygous

fibroblasts compared to untreated samples (Fig. 1B, 1C). However, significantly reduced

levels of the cleaved ATF6 cytosolic fragment were seen in homozygous $ATF6^{Y567N/Y567N}$

fibroblasts compared to heterozygous controls in response to experimental ER stress

induced by DTT (Fig. 1D). These findings showed that $ATF6$ mRNA and full-length

protein were normally generated in the $ATF6^{Y567N}$ mutant, but during ER stress, lower

levels of the functional transcriptional activator domain of ATF6 were present in

$ATF6^{Y567N/Y567N}$ fibroblasts despite normal-to-increased levels of full-length ATF6 protein

compared to heterozygous controls. Consistent with reduction of the ATF6

transcriptionally active fragment, we found reduced levels of $BiP/Grp78$ mRNA and

protein, an ER chaperone transcriptionally upregulated by ATF6 (Haze et al., 1999 and

Wang et al., 2000), in $ATF6^{Y567N/Y567N}$ fibroblasts compared to heterozygous controls in

response to experimental ER stress (Fig. 1E, 1F). These findings revealed that the

luminal ATF6[Y567N] mutation resulted in the impairment of ATF6 signaling in

$ATF6^{Y567N/Y567N}$ fibroblasts during ER stress.

ATF6 signaling is a key component of the Unfolded Protein Response (UPR) and

operates in parallel with signal transduction pathways controlled by the IRE1 and PERK

proteins to ensure normal ER function in mammalian cells(Water and Ron, 2011). We

next examined if the other branches of the UPR were also dysregulated in $ATF6^{Y567N/Y567N}$

fibroblasts. We assayed two specific molecular events of the IRE1 UPR signaling

pathway, *Xbp-1* mRNA splicing, an early proximal event specifically initiated by IRE1

activation (Calfon et al., 2002 and yoshida et al., 2001), and *ERdj4* transcription, a

downstream target gene induced by IRE1 signaling (Fig. 1E, 1G)(Wu et al., 2007,

Yamamoto et al., Shoulders et al., 2013). For the UPR signaling pathway regulated by

PERK, we examined levels of phosphorylated eIF2α protein, an early proximal event in

the PERK signal transduction pathway (Harding et al., 2000), and *CHOP* mRNA

transcript, a downstream target gene potently upregulated by PERK signaling (Fig. 1E,

1H) (Harding et al., 2000). For these IRE1 and PERK pathway markers, we observed a

small (<10%) but statistically significant decrease in *ERdj4* and *CHOP* transcript levels

between $ATF6^{Y567N/Y567N}$ fibroblasts and heterozygous controls (Fig. 1E, 1F, 1G, 1H).

These studies revealed that $ATF6^{Y567N/Y567N}$ fibroblasts with compromised ATF6 signaling

also showed mild impairment of other UPR pathways during ER stress.

Next, we investigated the mechanisms underlying the reduction in levels of the

cleaved ATF6 fragment observed during ER stress in $ATF6^{Y567N/Y567N}$ fibroblasts. To

ensure that the ATF6 protein level differences were not due to fibroblast cell line

differences, we expressed FLAG-tagged full-length wild-type ATF6 or mutant

ATF6[Y567N] in HEK293 cells. Similar to our findings in the primary patient

fibroblasts, we observed significantly reduced levels of cleaved ATF6 in response to ER

stress induced by DTT in cells expressing ATF6[Y567N] compared to wild-type ATF6

(Fig. 2A). In response to ER stress, full-length ATF6 traffics from ER to Golgi where the

Golgi-resident S1P and S2P proteases cleave the full-length molecule to liberate the

cytosolic transcriptional activator ATF6 fragment. We examined if defects in ER to

Golgi trafficking were responsible for the reduced production of cleaved ATF6 seen with

the ATF6[Y567N] mutant. First, we compared the sensitivity to Endoglycosidase H of

wild-type ATF6 and the ATF6[Y567N] mutant. Prior studies had demonstrated that

ATF6 was glycosylated with high mannose N-glycan in the ER, and this glycosylated

ATF6 isoform was sensitive to Endoglycosidase H (Haze et al., 1999 and Ye et al.,

2000). When ATF6 traveled to Golgi during ER stress, the high mannose N-glycan of

ATF6 was trimmed by glycosidases in the Golgi to produce an Endo H-resistant full

length ATF6 that could be transiently visualized by SDS-PAGE in cells before

undergoing S1P protease cleavage (Ye et al., 2000). We found that both wild type ATF6

and the mutant ATF6[Y567N] underwent glycosylation in the ER and showed identical

Endo H sensitivity profiles (Fig. 2B). However, when we added S1P inhibitor and

analyzed protein lysates collected from cells treated with DTT, we saw an Endo H-

resistant ATF6 isoform only with wild-type ATF6 (Fig. 2B). This finding provided

biochemical evidence that the mutant ATF6[Y567N] trafficked poorly from ER to Golgi

compared to the wild type protein during ER stress. Consistent with these biochemical

results, when we examined the subcellular localization of ATF6 by fluorescence confocal

microscopy, we found colocalization of wild-type ATF6 and the Golgi marker, GOLPH2,

in response to ER stress induced by DTT (Fig. 2C, left panels). However, the mutant

ATF6[Y567N] and GOLPH2 remained in separate subcellular compartments with no

colocalization of fluorescent signals under the same experimental conditions (Fig. 2C,

bottom two rows). We confirmed that both wild-type and mutant ATFg[Y567N] were

localized in the ER under resting (non-stressed) conditions as evident by colocalization

with the ER resident protein, PDI (Supplemental Figure 2). Another luminal domain mutant, ATF6[D564G], also showed impaired cleavage and trafficking in analogous assays (Fig. 2D,E). In sum, our studies revealed that the mechanism underlying attenuation of transcriptional activity in Class 1 ATF6 luminal domain mutants arose from an unexpected defect in ER to Golgi trafficking in response to ER stress, leading to reduced production of the cleaved transcriptional activator domain of ATF6.

Constitutive transcriptional activity in Class 2 ATF6 mutants.

The amino terminal domain of ATF6 is a 370-380 amino acid transcriptional factor of the basic-leucine zipper family, and expression of recombinant ATF6 fragments bearing only the first 373 amino acids from ATF6's cytosolic domain reconstituted the transcriptional activity of ATF6 in mammalian cells (Haze et al., 1999 and Chiang et al., 2012). Intriguingly, three of the *ATF6* mutations identified in achromatopsia patients were predicted to create ATF6 fragments of similar length to the ATF6(373) transcriptionally active fragment (Supplemental Figure 1 and (Kohl et al., 2015 and Xu et al., 2015)). To determine if this group of *ATF6* mutations showed functional activity, we expressed a recombinant FLAG-tagged ATF6 bearing a mutation that caused a valine to serine substitution at amino acid 371 of ATF6 followed by a stop codon three amino acids distally, ATF6[V371Sfs*3]. We found that the ATF6[V371Sfs*3] protein showed nearly identical size mobility to ATF6(373) in transfected HEK293 cells (Fig. 3A). We also found that ATF6[V371Sfs*3] transcriptionally induced ATF6 downstream target genes, GRP78/*BIP*, *HERPUDUD*1, and *SEL1L*, as potently as ATF6(373) (Bommiasamy et al., 2009) (Fig. 3B) . The expression of *CHOP* was also upregulated by both ATF6(373) and ATF6[V371Sfs*3] (Fig. 3B). These findings demonstrated that mutant

ATF6[V371Sfs*3] protein produces fully functional transcriptional activator *in vitro*. *In vivo*, the amount of functional truncated ATF6[V371Sfs*3] protein may be significantly less than wild-type ATF6 protein levels because the nonsense and premature stop codons found in these mutants may subject these mRNA transcripts to nonsense-mediated mRNA decay (Kohl et al., 2015).

Class 3 ATF6 mutants are transcriptionally inactive

Five *ATF6* mutations found in achromatopsia patients introduce nonsense or premature stop codons in exons encoding the cytosolic domain of ATF6 and are predicted to produce ATF6 cytosolic protein fragments with non-functional bZIP or lacking the entire bZIP and transcriptional activator domains (Supplemental Figure 1B, 1C, and (Kohl et al., 2015 and Ansar et al., 2015)). To test if this group of *ATF6* mutations compromised ATF6 function, we expressed recombinant FLAG-tagged ATF6 bearing several of these mutations including a proline to leucine mutation at position 118 followed by a premature stop codon 31 amino acids distally, ATF6[P118Lfs*31], which lacks the bZIP domain and part of the transcription activator domain, and a nonsense mutation of an asparagine residue at position 267, ATF6[N267*], which lacks only the bZIP domain. We detected protein expression of these truncated ATF6 mutants after transfection into HEK293 cells (Fig. 3A), but found no transcriptional induction of ATF6 target proteins with either mutant (Fig. 3A, 3B). Coupled with our prior studies of the ATF6[R324C] mutant (Kohl et al., 2015), these results identify a class of disease-associated *ATF6* mutations that cause loss of function through disruption of transcriptional activity by truncating the bZIP and/or transcriptional activator domains or by directly mutating critical residues in the bZIP domain in the ATF6 cytosolic domain.

To determine how loss of ATF6 activity affected other signaling arms of the UPR in patient cells with this class of mutations, we examined fibroblasts previously collected from a kindred expressing the ATF6[R324C] mutation (Kohl et al., 2015). These included an unaffected heterozygous parent ($ATF6^{R324C/+}$), proband #1, and three affected homozygous achromatic children ($ATF6^{R324C/R324C}$), patients # 2, #3, and #4 (Fig. 4A). We found comparable levels of $ATF6$ mRNA and full length ATF6 protein in heterozygous and homozygous fibroblasts (Fig. 4B, 4C). During experimentally induced ER stress conditions, we found increased levels of $ATF6$ mRNA and protein in heterozygous and homozygous fibroblasts (Fig. 4B, 4C). However, we found reduced levels of BiP/GRP78 protein in $ATF6^{R324C/R324C}$ fibroblasts compared to heterozygous controls in response to experimental ER stress consistent with our prior studies that showed that the ATF6[R324C] mutation compromised ATF6 signaling activity (Fig. 4C). This signaling defect arose from the impairment of the bZIP transcriptional activator domain itself, and not at earlier steps in the trafficking or production of the cytosolic ATF6 fragment, because full-length ATF6[R324C] protein underwent ER-to-Golgi trafficking (Figure 5B and 5C) and produced the cleaved ATF6 transcriptional activator fragment with similar kinetics to the wild-type protein in response to ER stress (Fig. 5A)

We next examined if the IRE1 and PERK signaling branches of the UPR were dysregulated in $ATF6^{R324C/R324C}$ fibroblasts. For IRE1 pathway markers, we saw no difference in $XBP1$ mRNA splicing between $ATF6^{R324C/R324C}$ fibroblasts and heterozygous control (Fig. 4D and Supplemental Figure 4). However, we saw significantly reduced transcriptional induction of $ERdj4$ in $ATF6^{R324C/R324C}$ fibroblasts compared to heterozygous control (Fig. 4D, 4E). For the PERK pathway markers, we saw no

difference in eIF2α phosphorylation between $ATF6^{R324C/R324C}$ fibroblasts and heterozygous control (Fig. 4C). However, we saw significantly reduced transcriptional induction of *CHOP* in $ATF6^{R324C/R324C}$ fibroblasts compared to heterozygous control (Fig. 4C, 4F). These studies revealed that $ATF6^{R324C/R324C}$ fibroblasts show compromised ATF6 transcriptional activity and also partial impairment of the IRE1 and PERK signaling branches of the UPR during ER stress.

Class 1 and Class 3 ATF6 mutant fibroblasts are more susceptible to ER stress-mediated cell death

Our studies revealed that Class 1 and Class 3 *ATF6* mutations both impaired ATF6 function. ATF6 ameliorates ER stress through its transcriptional induction of ER protein folding chaperones and enzymes. If ER stress is not alleviated, cells ultimately undergo cell death (Lin et al., 2007 and Rutkowski et al., 2006). We compared kinetics of cell death in patient fibroblasts expressing the Class 1 and Class 3 ATF6 mutants to see how loss of ATF6 function affected survival during extended ER stress. In response to thapsigargin exposure, we observed significantly increased levels of the apoptosis marker, cleaved Poly(ADP-ribose) Polymerase (PARP), in $ATF6^{Y567N/Y567N}$ fibroblasts compared to heterozygous controls (Fig. 5A, compare patient #3 fibroblasts with patients #1 and #2). Similarly, we observed increased levels of PARP cleavage in $ATF6^{R324C/R324C}$ fibroblasts compared to heterozygous parental control (Fig. 5B, compare patients #2, #3, and #4 with patient #1's cells). These studies revealed that a physiologic consequence of the loss of ATF6 function caused by Class 1 and Class 3 ATF6 mutations was heightened cell death in response to ER stress.

DISCUSSION

Our studies provide a framework for functional and pathomechanistic classification of *ATF6* mutations identified in achromatopsia (Fig. 6). Class I mutations affect the luminal domain of ATF6 and lead to loss of function. The pathomechanism underlying loss of function in Class 1 ATF6 mutations is inefficient trafficking from ER to Golgi during ER stress leading to poor production of the ATF6 transcriptional activator fragment (Supplemental Figure 1A). Class 2 mutations cluster near the transmembrane domain of ATF6. These mutations produce the entire cytosolic ATF6 fragment unbound to membrane and show fully intact ATF6 transcriptional activity (Supplemental Figure 1A). The Class 2 *ATF6* transcripts all bear premature stop codons and are likely targets of nonsense-mediated mRNA decay machinery (Kohl et al., 2015). Nonsense-mediated decay reduces mRNA transcript levels by ~50-85% depending on tissue type and environmental factors (Zetoune et al., 2008). Therefore, whether Class 2 mutations produce significant amounts of cytosolic ATF6 transcriptional activator fragment and show constitutive signaling *in vivo* requires further analysis in patients. Class 3 mutations affect the cytosolic domain of ATF6 and lead to loss of function. The pathomechanism underlying loss of function in this class of mutations is deletion or mutation of the bZIP and/or transcriptional activator domain.

Do the mechanistic differences we identified between *ATF6* mutations lead to phenotypic differences? In particular, we found that a Class 3 mutant had loss of ATF6 signaling plus partial impairment of IRE1 and PERK signaling (Fig. 4) while the Class 1 mutant only showed minor impairment of the transcriptional output of IRE1 and PERK signaling (Fig. 1). One possibility is that upregulation of ER stress genes, such as *ERdj4*

and *CHOP*, requires the production of functional ATF6 cytosolic bZIP transcriptional activator domain. In this view, Class 1 mutant ATF6 can still produce a functional cytosolic domain. This could explain why the upregulation of *ERdj4* and *CHOP* under ER stress is more severly impaired in Class 1 mutant ATF6s. Our identification of *ATF6* as a disease gene enables prospective longitudinal study of retinal structure and phenotype in patients with *ATF6* mutations to identify possible differences in achromatopsia disease phenotype and severity between different classes of *ATF6* mutations. Evaluation with adaptive optics and other retinal imaging modalities may reveal cone phenotype differences corresponding to different classes of *ATF6* mutations (Aboshiha et al., 2014 and Genead et al., 2011).

What are the therapeutic implications of differences between *ATF6* mutations' mechanisms of pathology? Class 1 ATF6 mutants inefficiently traffic from ER to Golgi but have normal bZIP transcriptional activator domains. For this class of mutations, our findings indicate that therapeutic strategies should focus on improving protein trafficking out of the ER so that the full-length ATF6 protein can be cleaved by the S1P and S2P Golgi-resident proteases. Once cleaved and separated from the defective luminal domain, the cytosolic ATF6 domain can engage in its normal transcriptional activator role. By contrast, the Class 3 ATF6 mutants require a different therapeutic approach than Class 1 trafficking mutants because Class 3 mutants completely lack or bear defective bZIP/transcriptional activator domains. Gene therapy to introduce functional ATF6 bZIP transcriptional activator or gene editing to repair the primary *ATF6* nucleotide alterations may be potential therapeutic strategies for patients with these types of *ATF6* mutations.

Our current study highlights the surprisingly diverse molecular defects in ATF6 activation caused by achromatopsia-associated mutations. Patient fibroblasts with several of these mutations showed increased sensitivity to ER stress-induced cell death and damage. Diverse environmental insults have been found to trigger ER stress in the eye including hypoxia, infection, inflammation, protein misfolding, and light damage (Kroeger et al., 2012, Yang et al., 2008, Nakanishi et al, 2013, Zhang et al., 2015, Zhang et al., 2014, Alavi et al., 2015, and Chiang et al., 2015). Exposure to these insults during retinal development may contribute to the cone dysfunction and vision loss that arises in children with mutations that compromise ATF6 function.

MATERIALS AND METHODS

Cell Culture

Human primary fibroblast cells or HEK293 cells were maintained at 37°C, 5% CO_2 in Dulbecco's modified Eagle medium (Mediatech, Manassas, VA) supplemented with 10% fetal calf serum (Mediatech), and 1% penicillin/streptomycin (Invitrogen, Carlsbad, CA). To induce ER stress, tunicamycin or thapsigargin (Calbiochem EMD Bioscience Inc, Darmstadt, Germany) were dissolved in DMF (Dimethylformamide) and DTT (Dithiothreitol) (BioPioneer Inc, San Diego, CA) was dissolved in water and added to the cell culture media at the indicated concentration.

Plasmid construction and transfection

To generate ATF6[P118Lfs*31], ATF6[N267*], and ATF6[V371Sfs*3] expression plasmid, mutation was introduced into FLAG-tag-ATF6(373).pcDNA3.1 plasmid by site-direct mutagenesis using overlapping PCR. To generate ATF6[Y567N] expression

plasmid, mutation was introduced into full length ATF6.pcDNA3.1 plasmid by site-direct mutagenesis using overlapping PCR. To express wild-type or mutant ATF6 in the cell culture system, plasmids containing the cDNA of those genes were transiently transfected to HEK293 using Lipofectamine 2000 (Invitrogen).

Molecular Biology

Cells were lysed and total RNA was collected using the RNeasy mini kit according to manufacturer's instructions (Qiagen, Hilden, Germany). mRNA was reverse-transcribed using the iScript cDNA Synthesis Kit (Bio-Rad, Hercules, CA). To analyze the level of *XBP1* mRNA splicing, cDNA was used as template for PCR amplification across the fragment of the *XBP1* cDNA bearing the intron target of IRE1's RNase activity. Primers used included: human *XBP1*, 5'-TTACGAGAGAAAACTCATGGC-3' and 5'- GGGTCCAAGTTGTCCAGAATGC-3'. PCR conditions were: 95°C for 5 min; 95°C for 1 min; 58°C for 30 sec; 72°C for 30 sec; 72°C for 5 min with 35 cycles of amplification. PCR products were resolved on a 2.5% agarose/1x TAE gel.

For quantitative PCR analysis, cDNA was used as template in SYBR green qPCR supermix (Bio-Rad). Primers used include: human *RPL19*, 5'-ATGTATCACAGCCTGTACCTG-3' and 5'-TTCTTGGTCTCTTCCTCCTTG-3'; human *GRP78*, 5'-GCCTGTATTTCTAGACCTGCC-3' and 5'-TTCATCTTGCCAGCCAGTTG-3'; human *HerpUD1*, 5′-AACGGCATGTTTTGCATCTG-3′ and 5′-GGGGAAGAAAGGTTCCGAAG-3′; human *Sel1L*, 5′-ATCTCCAAAAGGCAGCAAGC-3′ and 5′-TGGGAGAGCCTTCCTCAGTC-3′; human *Chop*, 5′-ACCAAGGGAGAACCAGGAAACG-3′ and 5′-TCACCATTCGGTCAATCAGAGC-3′;

human *ERdj4,* 5′-GGAAGGAGGAGCGCTAGGTC-3′ and 5′-

ATCCTGCACCCTCCGACTAC-3′; human ATF6, 5'-

GCTTTACATTCCTCCACCTCCTTG -3' and 5'- ATTTGAGCCCTGTTCCAGAGCAC

-3'; *Rpl19* mRNA levels served as internal normalization standards. qPCR condition was

95°C for 5 min; 95°C for 10 sec; 60°C for 10 sec; 72°C for 10 sec, with 40 cycles of

amplification.

Immunoblotting Analysis

Human fibroblasts or HEK293 cells expressing wild-type or mutant ATF6 were

lysed in SDS lysis buffer (2% SDS, 62.5 mM Tris-HCl pH 6.8, containing protease

inhibitors (Sigma-Aldrich), and phosphatase inhibitor (Thermo Scientific, Rockford, IL)).

Protein concentrations of the total cell lysates were determined by BCA protein assay

(Pierce, Rockford, IL). Equal amounts of protein were loaded onto 10% or 4-15% Mini-

PROTEAN TGX precast gels (Bio-Rad) and analyzed by Western blot. The following

antibodies and dilutions were used: anti-FLAG at 1:5000 (Sigma-Aldrich, St. Louis,

MO); anti-GFP at 1:1000 (Santa Cruz Biotechnologies, Santa Cruz, CA); anti-human

ATF6α antibody at 1:1000 (Abcam, Cambridge, MA); anti-phosph-eIF2α and anti-

cleaved PARP at 1:1000 (Cell Signaling, Danvers, MA); anti-BiP/GRP78 at 1:1000, anti-

GAPDH at 1:5000, anti-HSP90 at 1:5000, and anti-β-tubulin at 1:5000 (GeneTex Inc,

Irvine, CA). After overnight incubation with primary antibody, membranes were washed

in TBS with 0.1% Tween-20 (TBST) followed by incubation of a horseradish peroxidase-

coupled secondary antibody (Cell signaling, Danvers, MA). Immunoreactivity was

detected using the SuperSignal West chemiluminescent substrate (Pierce).

Endoglycosidase H (Endo H; New England Biolabs, Ipswich, MA) digestion was

performed on precleared total cell lysate for 1 hours at 37°C in the buffer supplied by the manufacturer. To preclear the cellular debris from the total lysate, cell lysate were spin at 15,000 rpm at 4°C for 1 hour.

Immunofluorescence and Confocal Microscopy

Cells were grown on poly-D-lysine coated glass cover slips and transfected with wild-type ATF6 or ATF6[Y567N]. For immunofluorescence analysis, cells were fixed for 20 minutes at room temperature in 4% Paraformaldehyde in PBS pH 7.4, washed briefly with PBS, and permeabilized with 0.1% Triton X-100 in PBS. Cells were then washed two times with 1% BSA in PBS and blocked with 5% goat serum in 1% BSA/PBS for 20 minutes. The cover slips were then incubated at room temperature for one hour with the mouse monoclonal anti-FLAG antibody (Sigma-Aldrich, St. Louis, MO) used at a dilution of 1:500, and the rabbit polyclonal anti-GOLPH2 antibody (GeneTex Inc, Irvine, CA) used at a dilution of 1:500. After washing in 0.1% BSA in PBS three times, cells were incubated with secondary antibodies. Secondary antibodies included Alexa546 goat anti-mouse (green) antibody (Molecular Probes, Invitrogen, Carlsbad, CA) and Alexa488 goat anti-rabbit (red) antibody (Molecular Probes, Invitrogen, Carlsbad, CA), and these were used at a dilution of 1:250. After washing in PBS three times, the cover slips were mounted in ProLong Gold antifade reagent with DAPI (Invitrogen, Carlsbad, CA), and images were collected with an Olympus FluoView-1000 confocal microscope and processed using Olympus FluoView Ver.2.0a Viewer software at the UCSD microscopy facility (www.microscopy.ucsd.edu).

ACKNOWLEDGMENTS

FIGURES AND LEGENDS

Figure 5. Impaired cleavage of ATF6 in response to ER stress in Class 1 mutant ATF6[Y567N] patient fibroblasts.(A) Pedigree of the family carrying ATF6 ^{Y567N} alleles. The heterozygous parents (ATF6 $^{Y567N/+}$) were indicated as patient # 1 and 2, for the mother and the father, respectively. The homozygous ☐(ATF6 $^{Y567N/Y567N}$) female child was indicated as patient #3. (B) ATF6 $^{Y567N/+}$ or ATF6 $^{Y567N/Y567N}$ patient fibroblasts were challenged with tunicamycin (TM) at the indicated concentration for 24 hours. mRNA was collected from the fibroblasts. ATF6 mRNA levels were measured by real-time quantitative PCR and normalized to the level in the untreated ATF6 $^{Y567N/+}$ parental control (#1) fibroblast cells.(C) Patient fibroblasts expressing ATF6[Y567N] were

challenged with tunicamycin at the indicated concentration for 24 hours. Endogenous ATF6 protein levels were detected by immunoblotting. The asterisk * shows the position of the deglycosylated full-length ATF6 protein ☐produced after tunicamycin treatment. (D) Patient fibroblasts expressing ATF6[Y567N] were challenged with DTT for 30 minutes and ATF6 protein levels were detected by immunoblotting using anti-ATF6 antibody. To help identify the electrophoretic migration patterns of full-length and cleaved ATF6 fragments, HEK293 cells were also challenged with DTT and lysates were immunoblotted with anti-ATF6 antibody. (E) Patient fibroblasts were challenged with tunicamycin at the indicated concentration for 24 hours. XBP1 mRNA splicing was assessed by RT-PCR. The level of phosphorylated-eIF2α and BiP/GRP78 were detected by immunoblotting. (F-H) The mRNA ☐levels of ATF6 downstream target gene, BIP/GRP78 (F), IRE1 downstream target gene, ERdj4 (G), and PERK downstream target gene, CHOP (H) were assessed by real-time quantitative PCR and normalized to mRNA levels in untreated samples.

A

ATF6^{Y567N/+} ATF6^{Y567N/+}

```
  [2]───┬───(1)
        │
   ┌────┴────┐
  (3)       ( )
```

ATF6^{Y567N/Y567N}

B

C

| Patient #: | 1 | 2 | 3 | 1 | 2 | 3 |
| TM (5μg/ml): | - | - | - | + | + | + |

95 kDa — *Full length ATF6

95 kDa — HSP90

D

| Patient #: | 1 | 2 | 3 | HEK |
| DTT (30 min): | - 1 2 | - 1 2 | - 1 2 | - 2 (mM) |

95 kDa — Full length ATF6

55 kDa — Cleaved ATF6

55 kDa — β-Tubulin

E

| Patient #: | 1 | 2 | 3 |
| TM (5μg/ml): | - + | - + | - + |

us / s — XBP-1

36 kDa — P-eIF2α

72 kDa — BiP/GRP78

95 kDa — HSP90

F

p=8.62X10^{-5}

p=0.0017

BIP/GRP78 mRNA level

Patient # : 1 2 3

G

p=0.019

p=0.002

ERdj4 mRNA level

Patient # : 1 2 3

H

p=0.010

p=0.008

CHOP mRNA level

Patient # : 1 2 3
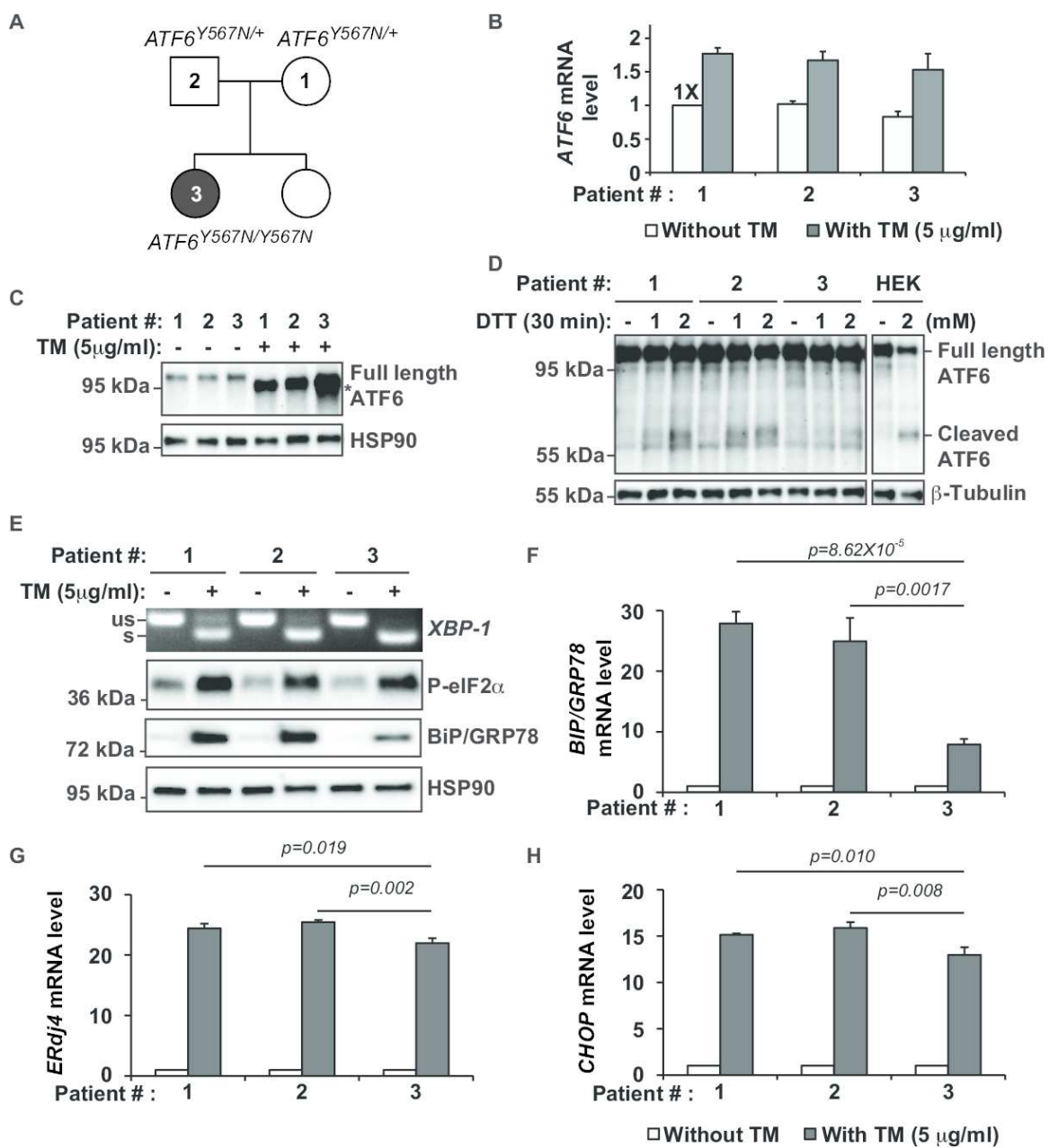
□ Without TM   ■ With TM (5 μg/ml)

45

Fig. 6. Impaired ER to Golgi transit of Class 1 mutant, ATF6[Y567N] and ATF6[D564G], during ER stress.

(A) Recombinant FLAG-tagged ATF6[Y567N] was expressed in HEK293 cells for 20 hours and then challenged with DTT as indicated. ATF6 protein levels were detected by immunoblotting with anti-FLAG. The band above 95 kDa and the band at 72 kDa represent the full length FLAG-tagged ATF6 and cleaved FLAG-tagged ATF6, respectively. (B) Recombinant FLAG-tagged wild type ATF6 and ATF6[Y567N] were expressed in HEK293 cells for 20 hours and then challenged with DTT with or without S1P inhibitor as indicated. Cell lysates were treated with Endo H as indicated. ATF6 protein levels were detected by immunoblotting with anti-FLAG. The bands above 95 kDa and the band at 72 kDa represent the full length FLAG-tagged ATF6 (either Endo H sensitive or insensitive) and cleaved FLAG-tagged ATF6, respectively. HSP90 levels were assessed as a loading control. (C) ATF6[Y567N] was expressed in HEK293 cells for 20 hours and then challenged with 2 mM of DTT for 40 minutes. The subcellular localization of ATF6 was visualized by immunofluorescence labeling and confocal microscopy by anti-FLAG antibody (shown in red). The Golgi apparatus was visualized by GOLPH2 immunostaining (shown in green). The nucleus was visualized by DAPI staining (shown in blue). The % of cells showing FLAG and GOLPH2 colocalization was quantified and shown in the bottom graph. Magnification bar, 10 μm. (D) Recombinant FLAG-tagged ATF6[D564G] was expressed in HEK293 cells for 20 hours and then challenged with DTT for 1 hour. ATF6 protein levels were detected by immunoblotting with anti-FLAG. (E) Recombinant FLAG-tagged wild type ATF6 and ATF6[D564G] were expressed in HEK293 cells for 20 hours and then challenged with DTT with or without S1P inhibitor as indicated for 90 minutes. Cell lysates were treated with Endo H as indicated.
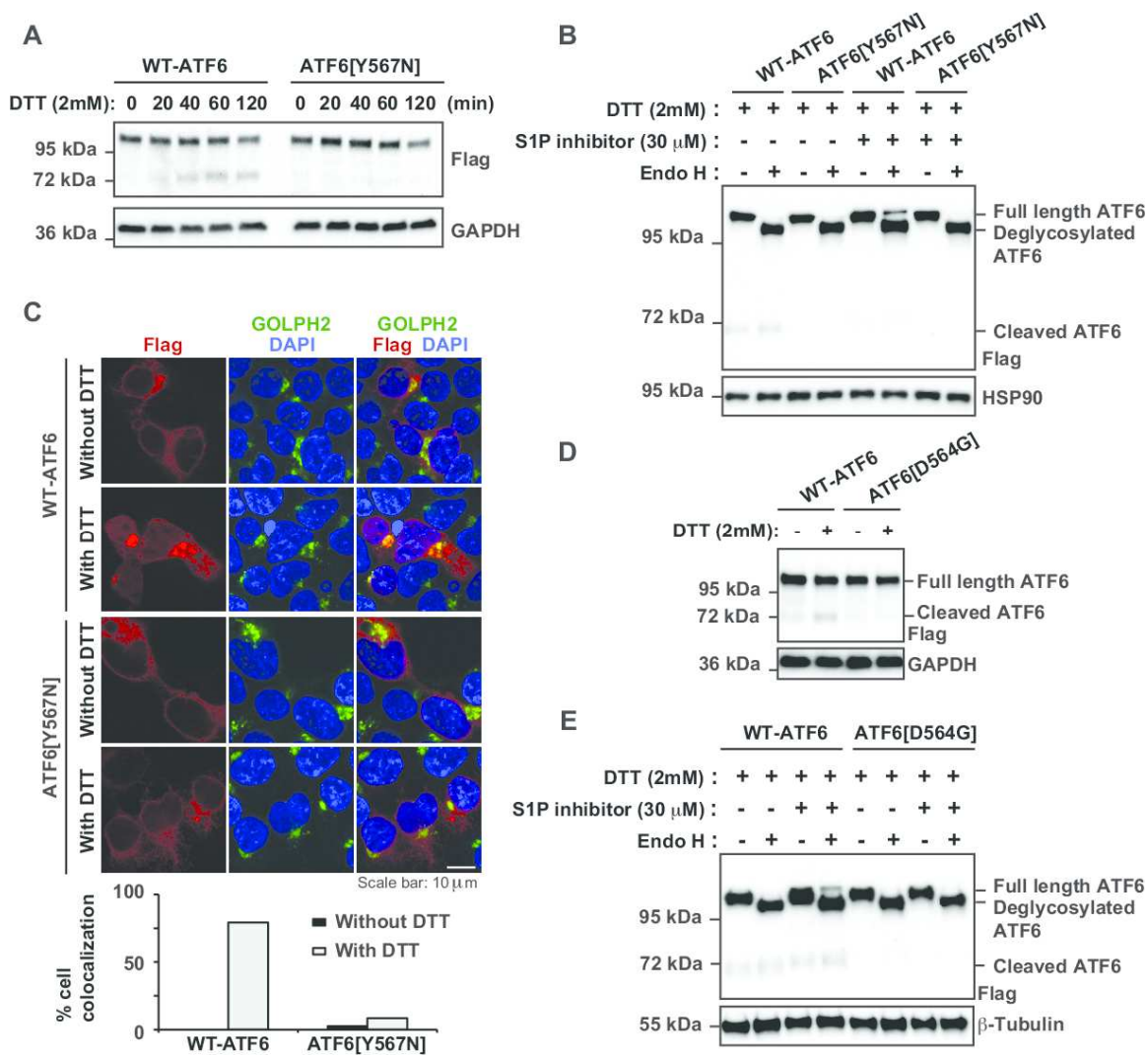
Scale bar: 10 μm

Figure 7. Transcriptional activator properties of Class 2 and Class 3 mutant ATF6 proteins.

(A) FLAG epitope-tagged ATF6(373), ATF6[V371Sfs*3] (a Class 2 mutant), and ATF6[P118Lfs*31] and ATF6[N267*] (Class 3 mutants) were co-transfected with GFP into HEK293 cells. ATF6 protein levels were detected by immunoblotting using anti-ATF6 and anti-FLAG antibodies. GRP78/BiP and GFP protein levels were detected by immunoblotting. HSP90 levels were assessed as a loading control. (B) ATF6(373), ATF6[P118Lfs*31], ATF6[N267*], and ATF6[V371Sfs*3] were expressed in the HEK293 cells and mRNA was collected. Levels of genes transcriptionally regulated by ATF6, including *BIP/GRP78, HERPUD1, and SEL1L* were measured by real-time quantitative PCR and normalized to levels in mock transfected cells. *CHOP,* a gene that is regulated by PERK activation, was also assessed.

A

B
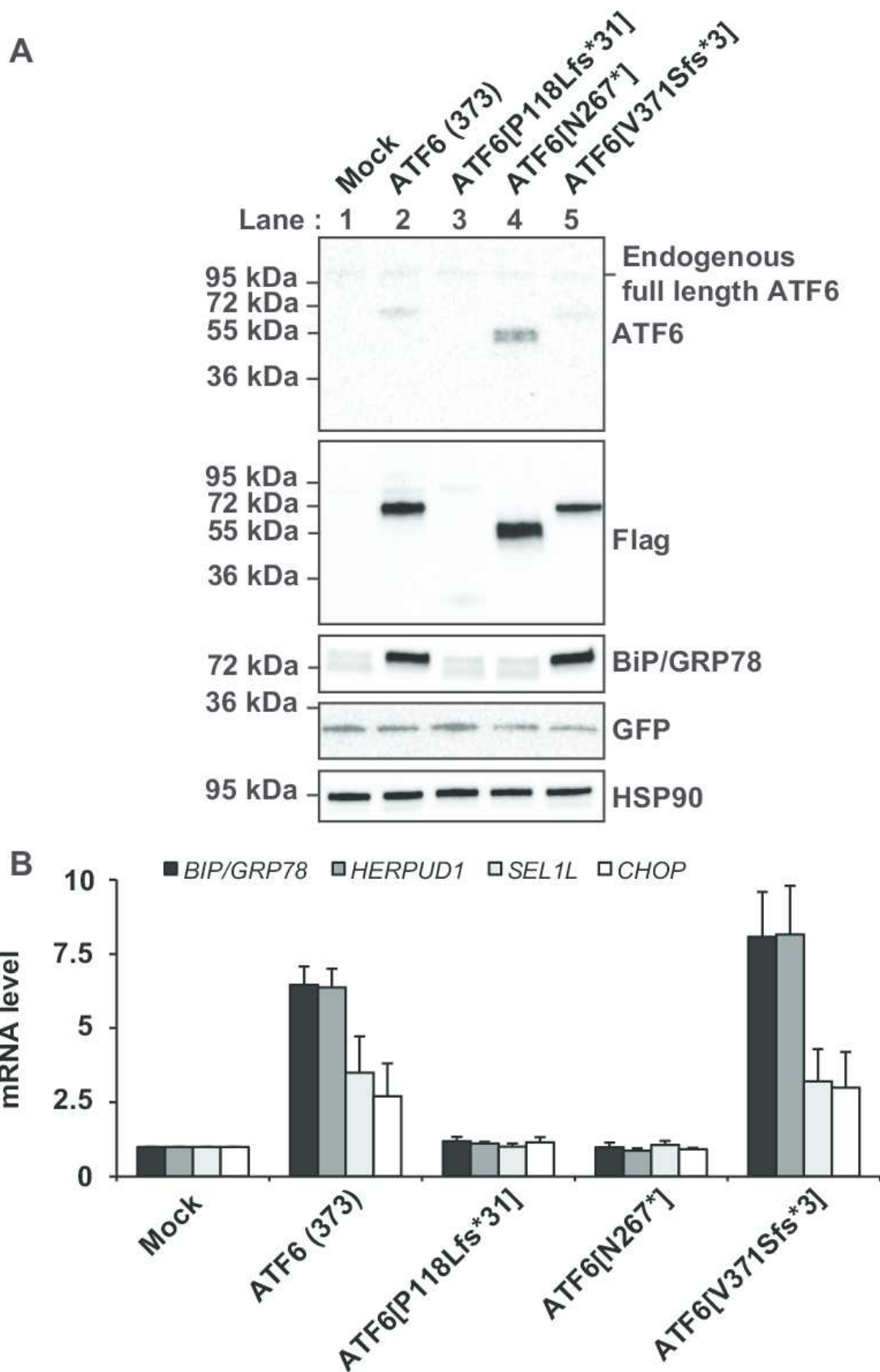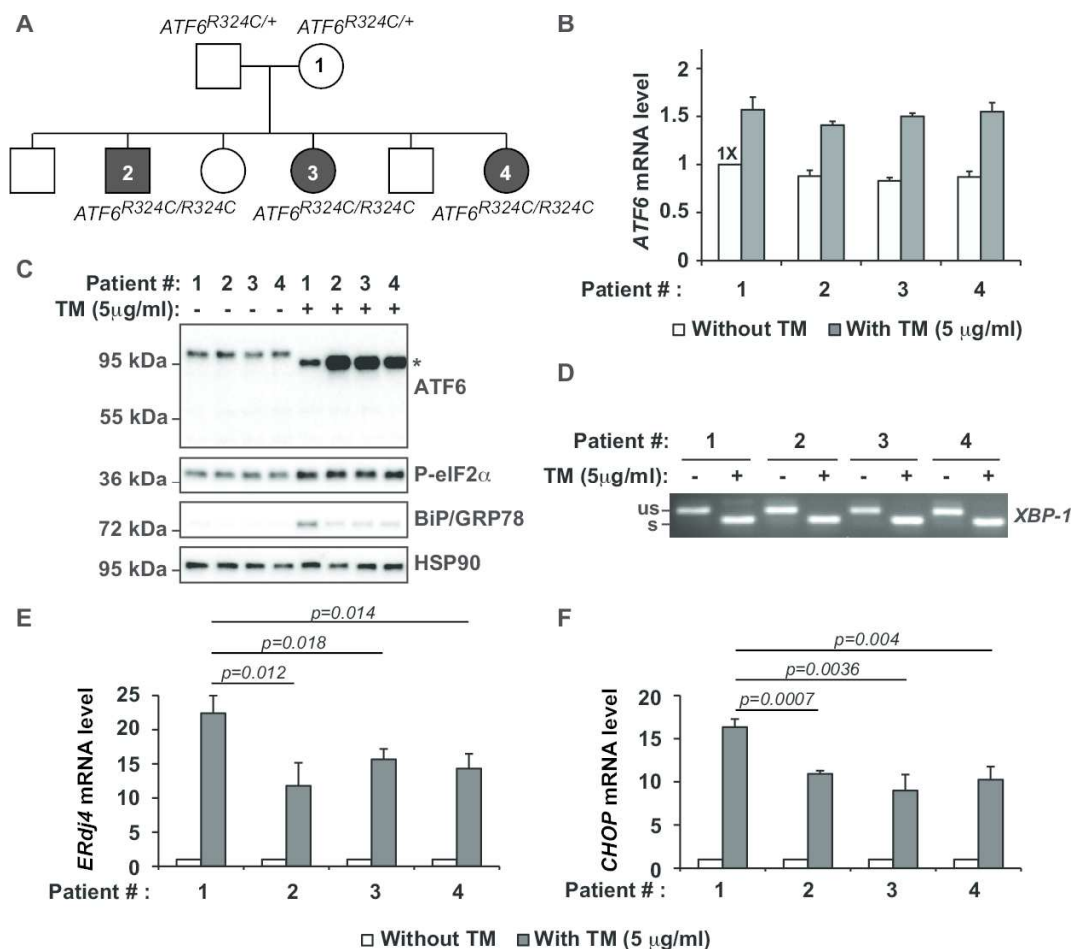
Figure 8. ATF6, IRE1, and PERK activity in Class 3 mutant, ATF6[R324C], patient fibroblasts.
(A) Pedigree of the family carrying $ATF6^{R324C}$ alleles. The heterozygous mother ($ATF6^{R324C/+}$) was indicated as patient # 1. The homozygous ($ATF6^{R324C/R324C}$) children were indicated as patient #2, 3, and 4. (B) $ATF6^{R324C/+}$ or $ATF6^{R324C/R324C}$ patient fibroblasts were challenged with tunicamycin at the indicated concentration for 24 hours. mRNA was collected from the fibroblasts. $ATF6$ mRNA levels were measured by real-time quantitative PCR and normalized to the level in the untreated $ATF6^{R324C/+}$ parental control (#1) fibroblast cells. (C) $ATF6^{R324C/+}$ or $ATF6^{R324C/R324C}$ patient fibroblasts were challenged with tunicamycin for 24 hours. ATF6, phosphorylated-eIF2α, and BiP/GRP78 were detected in protein lysates by immunoblotting. HSP90 levels were assessed as a loading control. (D) $XBP1$ mRNA splicing was visualized by semi-quantitative RT-PCR from patient fibroblasts treated with tunicamycin for 24 hours as indicated. (E and F) Patient fibroblasts were challenged with tunicamycin (TM) as indicated for 24 hours. The mRNA levels of IRE1 pathway downstream target gene, $ERdj4$ (E), and PERK pathway downstream target gene, $CHOP$ (F) were measured by real-time quantitative PCR and normalized to levels in untreated cells.
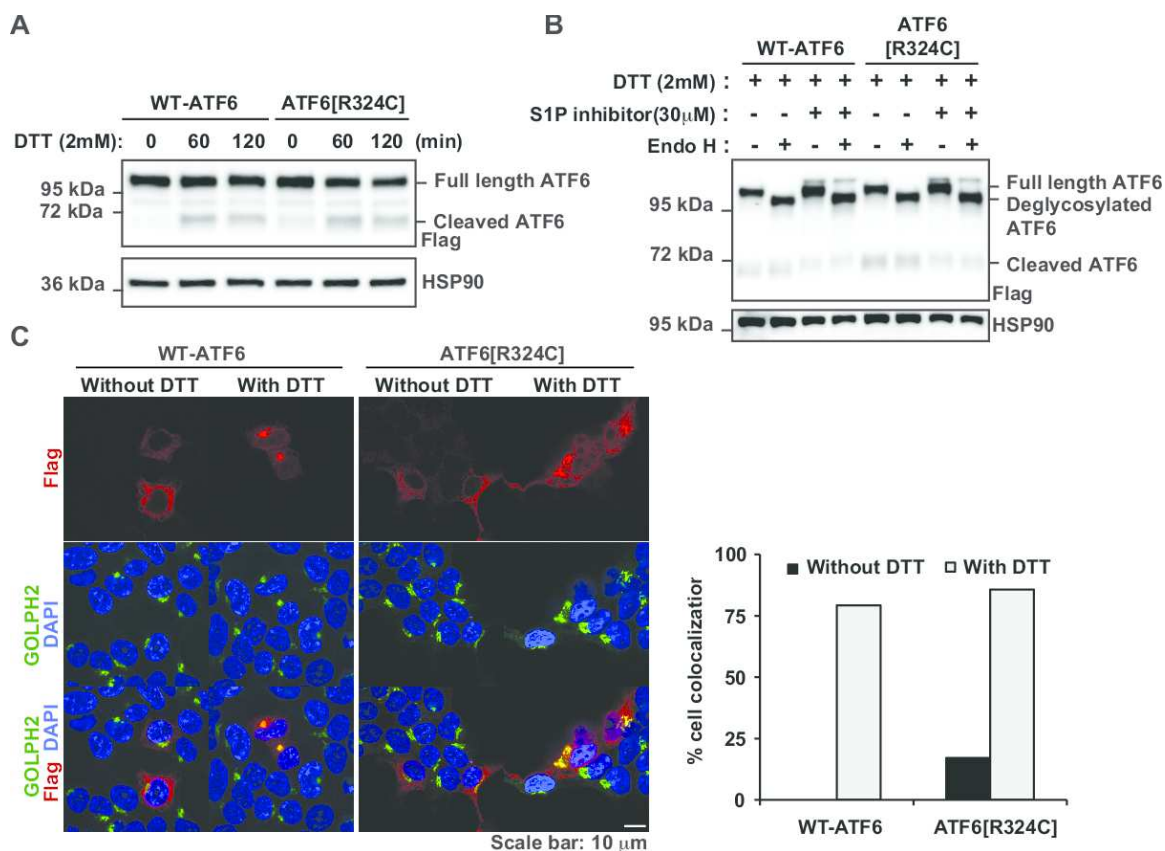
Figure 9. Normal ER to Golgi trafficking of Class 3 mutant, ATF6[R324C], during ER stress.
(A) Recombinant FLAG-tagged ATF6[R324C] was expressed in HEK293 cells for 20 hours and then challenged with DTT as indicated. ATF6 protein levels were detected by immunoblotting with anti-FLAG. (B) Recombinant FLAG-tagged wild type ATF6 and ATF6[R324C] were expressed in HEK293 cells for 20 hours and then challenged with DTT with or without S1P inhibitor as indicated for 90 minutes. Cells lysates were treated with Endo H as indicated. ATF6 protein levels were detected by immunoblottng with anti-FLAG. (C) ATF6[Y567N] was expressed in HEK293 cells for 20 hours and then challenged with 2 mM of DTT for 40 minutes. The subcellular localization of ATF6 was visualized by immunofluorescence labeling and confocal ⬜microscopy by anti-FLAG antibody (shown in red). The Golgi apparatus was ⬜visualized by GOLPH2 immunostaining (shown in green). The nucleus was ⬜visualized by DAPI staining (shown in blue). The % of cels showing FLAG and GOLPH2 colocalization with quantified and shown in the bottom grah. Maginification bar, 10 μm.
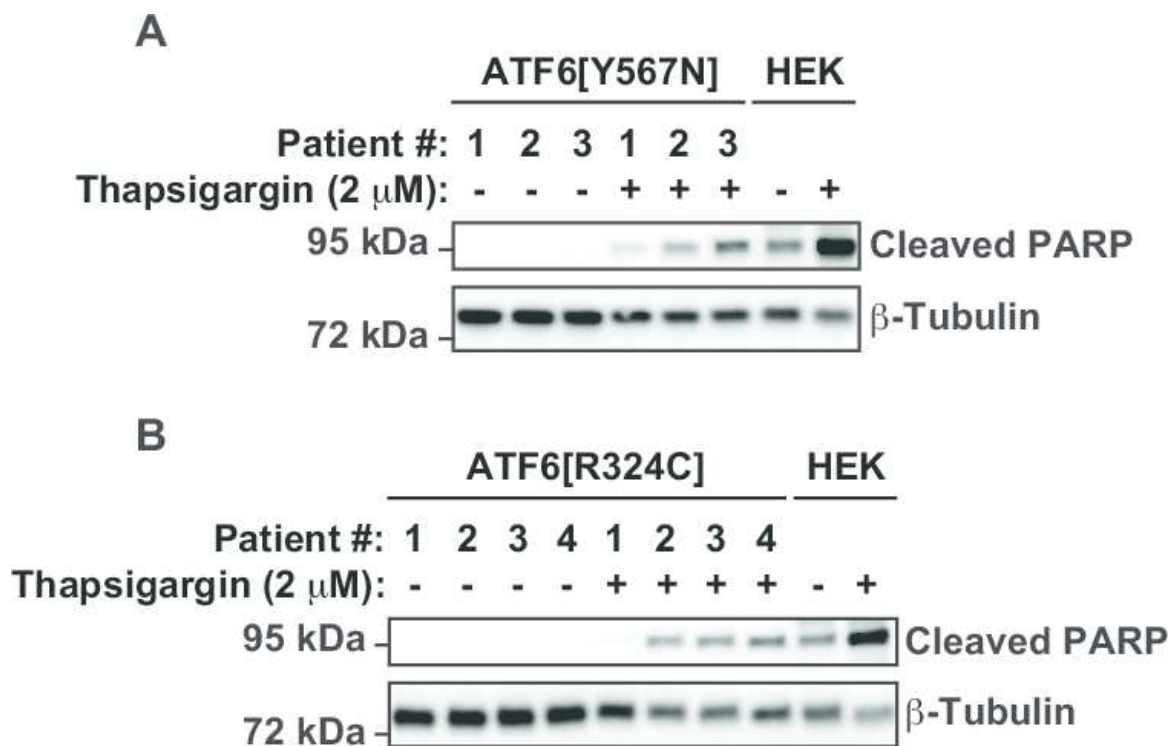
Figure 10. Class 1 or Class 3 mutant ATF6 fibroblasts show increases susceptibility to ER stress-induced cell death

Class 1 ATF6[Y567N/+] or ATF6 [Y567N/Y567N] human fibroblasts (A) and Class 3 ATF6 [+/R324C] or ATF6[R324C/R324C] human fibroblasts (B) were treated with thapsigargin at the indicated concentration for 3 □or 6 days, respectively. Cleaved PARP protein was detected by immunoblotting. As a control for the position of cleaved PARP protein, HEK293 cells were □treated with thapsigargin, and lysates were probed for PARP.

Chapter 2, in part, is a reprint of material that has been submitted for publication as it may appear in Proceedings of the National Academy of Sciences of the United States of America, 2016. Wei-Chieh Chiang, 2016. This thesis author was the secondary investigator and author of this paper.

Chapter 3 Role of ATF6 in the Degradation of P23H Rhodopsin Associated Retinitis Pigmentosa

3.1 Introduction

As previously mentioned, IRE1 and its downstream targets have been found to play a role in the clearance of mutant P23H rhodopsin protein, which is one of the most common mutations found to be responsible for the development of the retinal degenerative disease RP (Chiang et al., 2015). Besides this particular branch of the UPR, ATF6 has also been found to be associated with P23H rhodopsin. ATF6 was found to significantly reduce the levels of T17M, P23H, Y178C, C185R, D190G, K296E, and S334ter rhodopsin proteins in cells but had no effect on monomeric wildtype rhodopsin protein levels (Chiang et al., 2012). PERK, however, was found to not only target mutant rhodopsin but also wildtype rhodopsin and other proteins in the cell (Chiang et al., 2012).

Given these findings, I aimed to explore these findings further by studying how knocking out *ATF6* in P23H rhodopsin knock in mice can affect the rate of retinal degeneration and how it may affect the other two branches of the UPR, IRE1 and PERK. I hypothesize that knocking out *ATF6* will allow for the accumulation of mutant rhodopsin, therefore resulting in higher ER stress levels and an increase in the activation of IRE1 in order to relieve such levels of stress. Knocking out *ATF6*, however, should have little effect on PERK signaling given that that PERK did not appear to be selective in its degradation of mutant rhodopsin (Chiang et al., 2012).

3.2 Results

Generation of control ATF6$^{+/-}$ and experimental ATF6$^{-/-}$ mice carrying either Rho$^{+/+,}$
$^{+/P23H,}$ or P23H/P23H

In order to generate the control mice, *ATF6$^{+/+}$Rho$^{+/P23H}$* mice were crossed *ATF6^{-}*
$^{/-}$Rho$^{+/+}$ mice to yield mice that were predicted to be all *ATF6$^{+/-}$* and 50% Rho$^{+/+}$ and 50%

Rho$^{+/P23H}$ according to simple Mendelian principles (Figure 5A). Similarly we crossed

ATF6$^{+/+}$Rho$^{+/P23H}$ mice with *ATF6$^{-/-}$Rho$^{P23H/P23H}$* mice to yield mice that were all *ATF6$^{+/-}$*

and 50% *Rho$^{+/P23H}$* or 50% *Rho$^{P23H/P23H}$* (Figure 5B). I chose to use ATF6$^{+/-}$ mice as my

control for the interest of time given the mice available in our vivarium. Furthermore,

there is no significant difference in the phenotypes of *ATF6$^{+/-}$* and *ATF6$^{+/-}$*, which makes

using the *ATF6$^{-/-}$* model a viable option as a control.

In order to generate the experimental mice, I crossed *ATF6$^{-/-}$Rho$^{+/P23H}$* with *ATF6^{-}*
$^{/-}$Rho$^{+/+}$ mice, which should result in mice that are all *ATF6$^{-/-}$* and 50% *Rho$^{+/+}$* and 50%

Rho$^{+/P23H}$ (Figure 6A). I also crossed *ATF6$^{-/-}$Rho$^{+/P23H}$* with *ATF6$^{-/-}$Rho$^{+/P23H}$* mice, which

should result in mice that are all *ATF6$^{-/-}$* and 25% *Rho$^{+/+}$,* 50% *Rho$^{+/P23H}$*, and 25%

Rho$^{P23H/P23H}$ (Figure 6B). Lastly, I crossed *ATF6$^{-/-}$Rho$^{+/P23H}$* with *ATF6$^{-/-}$Rho$^{P23H/P23H}$*

mice, which should result in mice that are all *ATF6$^{-/-}$* and 50% *Rho$^{+/P23H}$* and 50%

Rho$^{P23H/P23H}$ (Figure 6C).

Knocking out ATF6 in Rho$^{P23H/P23H}$ increases XBP-1s mRNA levels in the retina

To determine the expression levels of various ER stress markers, I conducted

qPCR experiments on retinas of 12 day (P12) old mice. More specifically, I looked at the

levels of *Grp78/BiP, ERdj4, HerpUD1, Derl1, Sec24d, VCP, XBP1*-s, and *Chop*

expression. As predicted, there was no significant difference between the expression

levels of these genes examined when comparing between the control and experimental

mice under $Rho^{+/+}$ conditions (Figure 7A-H). Similarly, there was no significant

difference between the control and experimental animals when looking at mice that were

$Rho^{P23H/P23H}$ given that P23H rhodopsin is very degraded rapidly (Figure 7A-H) (Chiang

et al., 2015). However, when comparing between the control and experimental mice

under the $Rho^{+/P23H}$ background, there was a significant increase in the levels of XBP-1s

expression when ATF6 was not present (Figure 7G). The presence of more XBP-1s

mRNA indicates that there was more activation of IRE1 in the retinas of mice lacking

ATF6 (Chiang et al., 2015).

Knocking out ATF6 in $Rho^{P23H/P23H}$ increases BiP/Grp78 and IRE1 protein levels but

reduces clearance of rhodopsin in the retina

Next, to further investigate whether knocking out *ATF6* influences the

degradation of mutant rhodopsin and leads to the increase in the activation of IRE1, I

performed Western blot analyses on the retinas of P12 mice. As expected, I did not

observe noticeable differences in the amount of rhodopsin, BiP/Grp78, or IRE1a proteins

present between control $ATF6^{+/-}$ and experimental $ATF6^{-/-}$ mice that were under the

$Rho^{+/+}$ background given that there was no mutant rhodopsin present to be targeted for

degradation (Figure 8A). In the case of mice that were $Rho^{+/P23H}$, I saw an increase in the

amount of dimer and monomeric rhodopsin proteins present when *ATF6* was knocked out

(Figure 8B). There was also more Bip/Grp78 and IRE1a proteins in these retinas,

indicating there was more ER stress present and more activation of the UPR when *ATF6*

was not present (Figure B) (Morris et al., 1997 and Chiang et al., 2015). Lastly, when

examining mice of with the $Rho^{P23H/P23H}$ background, there was little to no rhodopsin

present in the retinas regardless of the presence of *ATF6* given that mutant rhodopsin is targeted for degradation very quickly (Figure 8C) (Chiang et al., 2015). In mice that were *ATF6*$^{+/-}$ there was more IRE1a protein present but there was more Bip/Grp78 present in the *ATF6*$^{-/-}$ mice (Figure 8C). These results do not suggest a difference in ER stress levels due to the lack of ATF6 when only mutant P23H rhodopsin is expressed in the retinas of these mice.

The mRNA levels of rhodopsin were similar between all genotypes, indicating that the differences seen in rhodopsin protein levels were not due lack of protein synthesis, but rather due to differences in protein degradation based on differences in genetic background (Figure 8D).

3.3 Discussion

ATF6 was found to play an important role in degrading a number of mutant rhodopsin proteins, one of which being P23H rhodopsin, while have no effect on wildtype rhodopsin (Chiang et al., 2012). To study how the loss ATF6 affects P23H rhodopsin degradation or ER stress levels in *in vivo* mouse models, I generated an experimental *ATF6$^{-/-}$* mouse line that were either *Rho$^{+/+, +/P23H, P23H/P23H}$* and a control mouse line that was *ATF6$^{+/-}$* and either *Rho$^{+/+, +/P23H, P23H/P23H}$*. Given that the P23H mutant rhodopsin is cleared from the retinas of mice very quickly and that retinal degeneration in *Rho$^{P23H/P23H}$* mice occurred as early as 12 days of life, I collected retinas from mice that were P10, P12, and P15 in order to not only compare the affects of knocking out *ATF6* in the same age group but to also determine whether knocking this gene out affects the rate of retinal degeneration (Chiang et al., 2015).

In the first set of studies that I performed on P12 mouse retinas, I found that the mRNA expression levels of UPR downstream targets were not increased nor decreased significantly when *ATF6* is knocked out. However, XBP-1s was the one gene that was found to be upregulated in response to knocking out *ATF6* but only when it was under a *Rho$^{+/P23H}$* background (Figure 5G). The increase in expression of XBP-1s suggests that IRE1 is more active when ATF6 is not present and could be compensating for the loss of a branch of the UPR that can be used to target mutant rhodopsin accumulation (Figure 6G). Similarly, when looking at rhodopsin, BiP/Grp78, and IRE1a protein levels, I found that mice that were *ATF6$^{-/-}$Rho$^{+/P23H}$* had not only more monomeric and dimer rhodopsin present but also had an increase in the presence of BiP/Grp78 and IRE1a. This indicates that without *ATF6*, there was more ER stress present in the retina but rhodopsin could be

preserved through the increased activation of the IRE1a (Figure 7B). When I measured the mRNA levels of rhodopsin present in all lines of mice, there was no difference in the amount of rhodopsin present meaning that the presence or lack of rhodopsin was not due to differences in expression but due to more or less protein degradation (Figure 7D).

The next steps in this study will be to determine if I can see similar trends in mRNA and protein levels in mice of the same background at both P10 and P15. Also, histology experiments will be necessary in order to visual retinal degeneration or lack of due to knocking out *ATF6*.

3.4 Material and Methods

Animals

Breeding pairs of P23H rod opsin knock-in and ATF6 knock out mice were maintained generate control and experimental mice as described above (Sakami et al., 2011 and Wu et al., 2007). C57BL/6J mice were used as wild-type controls ($ATF6^{+/+}$ or $Rho^{+/+}$). Mice were maintained in a barrier animal facility in a 12:12 light cycle at in-cage irradiance of less than 125 lux and provided standard mouse chow (UCSD). Retinal tissues were collected from the animals of either sex for 12 days of age. The UCSD Animal Care staff checked mice daily. In addition, laboratory personnel checked births in the morning and evening during the light phase of the light cycle to determine exact birthdates because early eye developmental and degenerative events occurred rapidly once they commenced. All animal studies followed the guidelines of the institutional animal care committees at UCSD and were conducted in accordance with the recommendations of the American Veterinary Medical Association Panel on Euthanasia and the Association of Research for Vision and Ophthalmology.

Tissue Harvesting

Immediately after euthanizing mice, the eyes of each mouse was removed, and the retina was dissected by the Winkling procedure and rapidly frozen in liquid nitrogen for biochemical and molecular analyses (Winkler, 1972).

Molecular Biology

Retinas were lysed and total RNA was collected with a RNeasy mini kit (Qiagen, Germany). mRNA was reverse-transcribed with the iScript cDNA Synthesis Kit (Bio-Rad, Hercules, CA). For quantitative PCR analyses, primers included:

mouse *rhodopsin* mRNA, 5′-TTCACCACCACCCTCTACACATCAC-3′ and 5′-

CGGAAGTTGCTCATCGGCTTG-3′; mouse *Xbp-1s* mRNA, 5′-

GAGTCCGCAGCAGGTG-3′ and 5′-GTGTCAGAGTCCATGGGA-3′;

mouse *Derl1* mRNA, 5′-CGCGATTTAAGGCCTGTTAC-3′ and 5′-

GGTAGCCAGCGGTACAAAAA-3′; mouse *VCP* mRNA, 5′-

AAGTCCCCAGTTGCCAAGGATG-3′ and 5′-AGCCGATGGATTTGTCTGCCTC-3′;

mouse *ERdj4*, 5′-TAAAAGCCCTGATGCTGAAGC -3′ and 5′-

TCCGACTATTGGCATCCGA -3′; mouse *Grp78/BiP*: 5′-

CCTGCGTCGGTGTGTTCAAG-3′ and 5′-AAGGGTCATTCCAAGTGCG-3′; mouse

Rpl19: 5′-ATGCCAACTCCCGTCAGCAG- 3′ and 5′-

TCATCCTTCTCATCCAGGTCACC-3′; mouse *Chop*: 5′-

ACGGAAACAGAGTGGTCAGTGC-3′ and 5′-CAGGAGGTGATGCCCACTGTTC-3′;

mouse *HerpUD1*: 5'-ACCGCAGTTGGAGTGTGAGTCG-3' and 5'-

TCTGGCATTTTGGAGGGATTCTTC-3'; and mouse *Sec24d*: 5'-

TCTTTGCCTACTGCCGAAGCAC-3' and 5'-GACCCAAGGAAGCCACATCCAC-3'.

For all qPCR analysis, *RPL19* mRNA levels, a transcript with levels unaltered by ER

stress, served as internal normalization standards. qPCR conditions were 95°C for 5 min;

95°C for 10 sec; 60°C for 10 sec; 72°C for 10 sec, with 50 cycles of amplification.

Immunoblotting Analyses

Retinas from 3 to 5 mice were collected from $ATF6^{+/-}Rho^{+/+}$, $ATF6^{+/-}Rho^{P23H/+}$,

$ATF6^{+/-}Rho^{P23H/P23H}$ mice, $ATF6^{-/-}Rho^{+/+}$, $ATF6^{-/-}Rho^{P23H/+}$, and $ATF6^{-/-}Rho^{P23H/P23H}$ mice.

Mouse retinas were lysed in 200 μl of lysis buffer (PBS, 0.5 g/ml n-dodecyl-b-D-

maltoside (Calbiochem EMD Bioscience), protease inhibitors (Sigma-Aldrich), and

phosphatase inhibitor (Thermo Scientific, Rockford, IL)). The following antibodies and dilutions were used: B630N anti-rhodopsin 1:1000 (gift of W.C. Smith, Gainesville, FL); anti-BiP/GRP78 at 1:1000, anti-IRE1a at 1:1000 and anti-HSP90 at 1:1000 (GeneTex). After overnight incubation with primary antibody, membranes were washed followed by incubation with a horseradish peroxidase-coupled secondary antibody (Cell signaling). Immunoreactivity was detected with the SuperSignal West chemiluminescent substrate (Pierce).

Statistical Analyses

All results are presented as means ± standard deviations from 3 mice per experimental condition as indicated. Student two-tailed *t*-tests (for paired samples) were performed to determine *p*-values. A *p* value of ≤0.05 was considered statistically significant.

3.5 Figures

A

$ATF6^{-/-}Rho^{+/+}$

$ATF6^{+/+}Rho^{+/P23H}$

	$ATF6^-$ Rho^+	$ATF6^-$ Rho^+	$ATF6^-$ Rho^+	$ATF6^-$ Rho^+
$ATF6^+$ Rho^+	$ATF6^{+/-}$ $Rho^{+/+}$	$ATF6^{+/-}$ $Rho^{+/+}$	$ATF6^{+/-}$ $Rho^{+/+}$	$ATF6^{+/-}$ $Rho^{+/+}$
$ATF6^+$ Rho^{P23H}	$ATF6^{+/-}$ $Rho^{+/P23H}$	$ATF6^{+/-}$ $Rho^{+/P23H}$	$ATF6^{+/-}$ $Rho^{+/P23H}$	$ATF6^{+/-}$ $Rho^{+/P23H}$
$ATF6^+$ Rho^+	$ATF6^{+/-}$ $Rho^{+/+}$	$ATF6^{+/-}$ $Rho^{+/+}$	$ATF6^{+/-}$ $Rho^{+/+}$	$ATF6^{+/-}$ $Rho^{+/+}$
$ATF6^+$ Rho^{P23H}	$ATF6^{+/-}$ $Rho^{+/P23H}$	$ATF6^{+/-}$ $Rho^{+/P23H}$	$ATF6^{+/-}$ $Rho^{+/P23H}$	$ATF6^{+/-}$ $Rho^{+/P23H}$

Total Crossings: 1

Expected Ratios:
$ATF6^{+/-}Rho^{+/+}$: 1/2
$ATF6^{+/-}Rho^{+/P23H}$:1/2

B

$ATF6^{-/-}Rho^{+/P23H}$

$ATF6^{+/+} Rho^{P23H/P23H}$

	$ATF6^-$ Rho^+	$ATF6^-$ Rho^{P23H}	$ATF6^-$ Rho^+	$ATF6^-$ Rho^{P23H}
$ATF6^+$ Rho^{P23H}	$ATF6^{+/-}$ $Rho^{+/P23H}$	$ATF6^{+/-}$ $Rho^{P23H/P23H}$	$ATF6^{+/-}$ $Rho^{+/P23H}$	$ATF6^{+/-}$ $Rho^{P23H/P23H}$
$ATF6^+$ Rho^{P23H}	$ATF6^{+/-}$ $Rho^{+/P23H}$	$ATF6^{+/-}$ $Rho^{P23H/P23H}$	$ATF6^{+/-}$ $Rho^{+/P23H}$	$ATF6^{+/-}$ $Rho^{P23H/P23H}$
$ATF6^+$ Rho^{P23H}	$ATF6^{+/-}$ $Rho^{+/P23H}$	$ATF6^{+/-}$ $Rho^{P23H/P23H}$	$ATF6^{+/-}$ $Rho^{+/P23H}$	$ATF6^{+/-}$ $Rho^{P23H/P23H}$
$ATF6^+$ Rho^{P23H}	$ATF6^{+/-}$ $Rho^{+/P23H}$	$ATF6^{+/-}$ $Rho^{P23H/P23H}$	$ATF6^{+/-}$ $Rho^{+/P23H}$	$ATF6^{+/-}$ $Rho^{P23H/P23H}$

Total Crossings: 2

Expected Ratios:
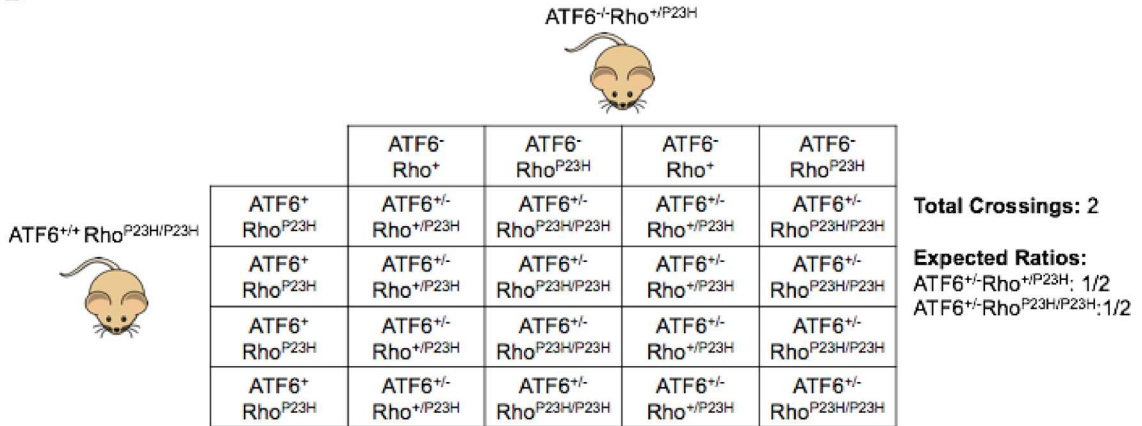$ATF6^{+/-}Rho^{+/P23H}$: 1/2
$ATF6^{+/-}Rho^{P23H/P23H}$:1/2

Figure 11. A simple Mendelian cross to generate $ATF6^{+/-}$ control mice that are $Rho^{+/+, +/P23H, or P23/P23H}$

(A) Two breeding pairs worth of mice that were $ATF6^{+/+}Rho^{+/P23H}$ and $ATF6^{-/-}Rho^{+/+}$ were crossed to yield two different possible control genotypes for analysis. All the offspring should be $ATF6^{+/-}$ but half will be $Rho^{+/+}$ and the other half will be $Rho^{+/P23H}$.
(B) Two breeding pairs worth of mice that were $ATF6^{+/+}Rho^{P23H/P23H}$ and $ATF6^{-/-}Rho^{+/P23H}$ were crossed to yield two different possible control genotypes for analysis. All the offspring should be $ATF6^{+/-}$ but half will be $Rho^{+/P23H}$ and the other half will be $Rho^{P23H/P23H}$.

Figure 12. A simple Mendelian cross to generate $ATF6^{-/-}$ experimental mice that are $Rho^{+/+,\ +/P23H,\ or\ P23/P23H}$

A) Two breeding pairs worth of mice that were $ATF6^{-/-}Rho^{+/P23H}$ and $ATF6^{-/-}Rho^{+/+}$ were crossed to yield two different possible experimental genotypes for analysis. All the offspring should be ATF6$^{-/-}$ but half will be $Rho^{+/+}$ and the other half will be $Rho^{+/P23H}$. (B) Two breeding pairs worth of mice that were $ATF6^{-/-}Rho^{+/P23H}$ and $ATF6^{-/-}Rho^{+/P23H}$ were crossed to yield three different possible experimental genotypes for analysis. All the offspring should be ATF6$^{-/-}$ but a quarter will be $Rho^{+/+}$, half will be $Rho^{+/P23H}$, and the last quarter will be $Rho^{P23H/P23H}$. (C) Three breeding pairs worth of mice that were $ATF6^{-/-}Rho^{P23H/P23H}$ and $ATF6^{-/-}Rho^{P23H/P23H}$ were crossed to yield two different possible experimental genotypes for analysis. All the offspring should be ATF6$^{-/-}$ but half will be $Rho^{+/P23H}$ and the other half will be $Rho^{P23H/P23H}$.

A

ATF6$^{-/-}$Rho$^{+/+}$

ATF6$^{-/-}$Rho$^{+/P23H}$

	ATF6$^-$ Rho$^+$	ATF6$^-$ Rho$^+$	ATF6$^-$ Rho$^+$	ATF6$^-$ Rho$^+$
ATF6$^-$ Rho$^+$	ATF6$^{-/-}$ Rho$^{+/+}$	ATF6$^{-/-}$ Rho$^{+/+}$	ATF6$^{-/-}$ Rho$^{+/+}$	ATF6$^{-/-}$ Rho$^{+/+}$
ATF6$^-$ Rho^{P23H}	ATF6$^{-/-}$ Rho$^{+/P23H}$	ATF6$^{-/-}$ Rho$^{+/P23H}$	ATF6$^{-/-}$ Rho$^{+/P23H}$	ATF6$^{-/-}$ Rho$^{+/P23H}$
ATF6$^-$ Rho$^+$	ATF6$^{-/-}$ Rho$^{+/+}$	ATF6$^{-/-}$ Rho$^{+/+}$	ATF6$^{-/-}$ Rho$^{+/+}$	ATF6$^{-/-}$ Rho$^{+/+}$
ATF6$^-$ Rho^{P23H}	ATF6$^{-/-}$ Rho$^{+/P23H}$	ATF6$^{-/-}$ Rho$^{+/P23H}$	ATF6$^{-/-}$ Rho$^{+/P23H}$	ATF6$^{-/-}$ Rho$^{+/P23H}$

Total Crossings: 2

Expected Ratios:
ATF6$^{-/-}$Rho$^{+/+}$: 1/2
ATF6$^{-/-}$Rho$^{+/P23H}$:1/2

B

ATF6$^{-/-}$ Rho$^{+/P23H}$

ATF6$^{-/-}$ Rho$^{+/P23H}$

	ATF6$^-$ Rho$^+$	ATF6$^-$ Rho^{P23H}	ATF6$^-$ Rho$^+$	ATF6$^-$ Rho^{P23H}
ATF6$^-$ Rho$^+$	ATF6$^{-/-}$ Rho$^{+/+}$	ATF6$^{-/-}$ Rho$^{+/P23H}$	ATF6$^{-/-}$ Rho$^{+/+}$	ATF6$^{-/-}$ Rho$^{+/P23H}$
ATF6$^-$ Rho^{P23H}	ATF6$^{-/-}$ Rho$^{+/P23H}$	ATF6$^{-/-}$ Rho$^{P23H/P23H}$	ATF6$^{-/-}$ Rho$^{+/P23H}$	ATF6$^{-/-}$ Rho$^{P23H/P23H}$
ATF6$^-$ Rho$^+$	ATF6$^{-/-}$ Rho$^{+/+}$	ATF6$^{-/-}$ Rho$^{+/P23H}$	ATF6$^{-/-}$ Rho$^{+/+}$	ATF6$^{-/-}$ Rho$^{+/P23H}$
ATF6$^-$ Rho^{P23H}	ATF6$^{-/-}$ Rho$^{+/P23H}$	ATF6$^{-/-}$ Rho$^{P23H/P23H}$	ATF6$^{-/-}$ Rho$^{+/P23H}$	ATF6$^{-/-}$ Rho$^{P23H/P23H}$

Total Crossings: 2

Expected Ratios:
ATF6$^{-/-}$Rho$^{+/+}$: 1/4
ATF6$^{-/-}$Rho$^{+/P23H}$:1/2
ATF6$^{-/-}$Rho$^{P23H/P23H}$:1/4

C

ATF6$^{-/-}$Rho$^{P23H/P23H}$

ATF6$^{-/-}$Rho$^{+/P23H}$

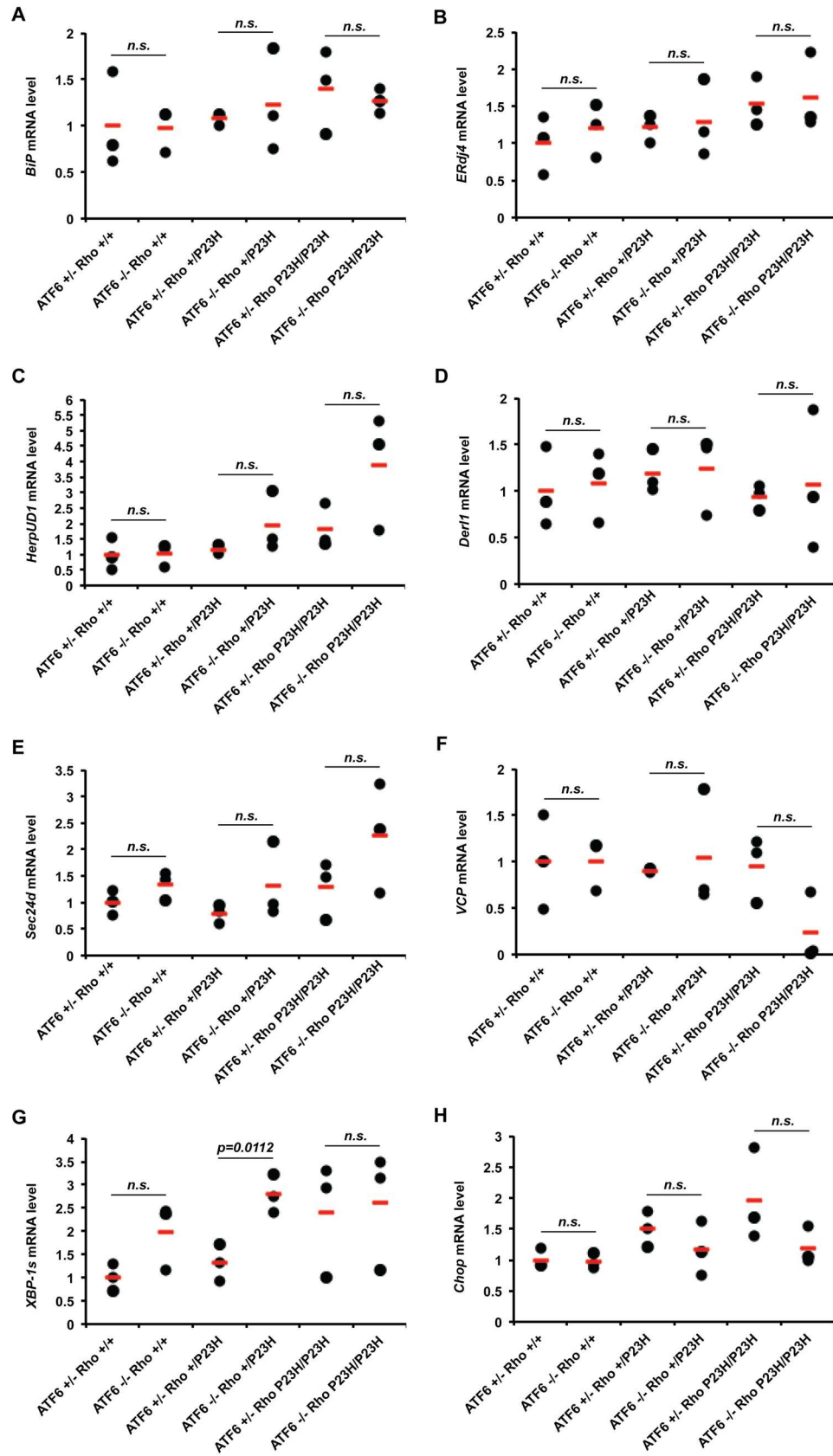|	ATF6$^-$ Rho^{P23H}	ATF6$^-$ Rho^{P23H}	ATF6$^-$ Rho^{P23H}	ATF6$^-$ Rho^{P23H}
ATF6$^-$ Rho$^+$	ATF6$^{-/-}$ Rho$^{+/P23H}$	ATF6$^{-/-}$ Rho$^{+/P23H}$	ATF6$^{-/-}$ Rho$^{+/P23H}$	ATF6$^{-/-}$ Rho$^{+/P23H}$
ATF6$^-$ Rho^{P23H}	ATF6$^{-/-}$ Rho$^{P23H/P23H}$	ATF6$^{-/-}$ Rho$^{P23H/P23H}$	ATF6$^{-/-}$ Rho$^{P23H/P23H}$	ATF6$^{-/-}$ Rho$^{P23H/P23H}$
ATF6$^-$ Rho$^+$	ATF6$^{-/-}$ Rho$^{+/P23H}$	ATF6$^{-/-}$ Rho$^{+/P23H}$	ATF6$^{-/-}$ Rho$^{+/P23H}$	ATF6$^{-/-}$ Rho$^{+/P23H}$
ATF6$^-$ Rho^{P23H}	ATF6$^{-/-}$ Rho$^{P23H/P23H}$	ATF6$^{-/-}$ Rho$^{P23H/P23H}$	ATF6$^{-/-}$ Rho$^{P23H/P23H}$	ATF6$^{-/-}$ Rho$^{P23H/P23H}$

Total Crossings: 3

Expected Ratios:
ATF6$^{-/-}$Rho$^{+/P23H}$: 1/2
ATF6$^{-/-}$Rho$^{P23H/P23H}$:1/2

Figure 13. Loss of *ATF6* in *Rho*$^{+/P23H}$ mice increases expression of *XBP-1s* but not other UPR Downstream Targets

(A) *BiP*, (B) *ERdj4*, (C) *HerpUD1*, (D) *Derl1*, (E) *Sec24d*, (F) *VCP*, (G) *XBP-1s*, and (H) *Chop* mRNA levels were quantified in the retinas of *ATF6*$^{-/-}$ *Rho*$^{+/+}$, *ATF6*$^{-/-}$*Rho*$^{P23H/+}$, and *ATF6*$^{-/-}$*Rho*$^{P23H/P23H}$ mice and are shown relative to levels in age-matched control *ATF6*$^{+/-}$*Rho*$^{+/+}$, *ATF6*$^{+/-}$*Rho*$^{P23H/+}$, and *ATF6*$^{+/-}$*Rho*$^{P23H/P23H}$.

SDs are based on measurements from at least three mice of each genotype at P12.
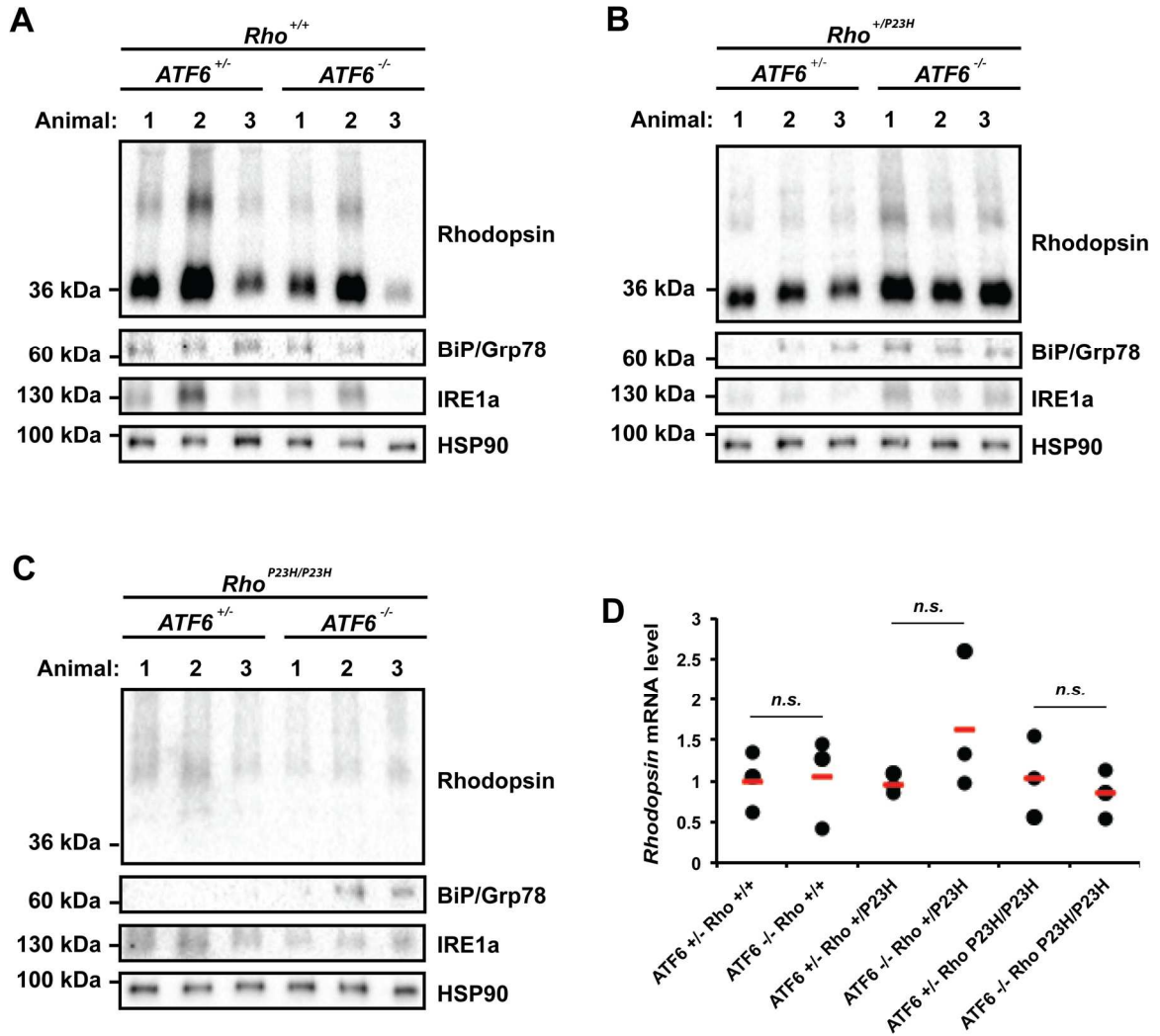
Figure 14. Loss of *ATF6* in *Rho*^{+/P23H} mice increases rhodopsin and increases BiP/Grp78 and IRE1a protein levels

Retinal protein lysates were collected from (A) $ATF6^{+/-}Rho^{+/+}$ and $ATF6^{-/-}Rho^{+/+}$, (B) $ATF6^{+/-}Rho^{P23H/+}$ and $ATF6^{-/-}Rho^{P23H/+}$, and (C) $ATF6^{+/-}Rho^{P23H/P23H}$ and $ATF6^{-/-}Rho^{P23H/P23H}$ mice at P12. Rhodopsin, BiP/Grp78, and IRE1a were detected by immunoblotting. HSP90 protein levels served as a loading control. (D) *Rhodopsin* mRNA levels were quantified in the retinas of $ATF6^{-/-}Rho^{+/+}$, $ATF6^{-/-}Rho^{P23H/+}$, and $ATF6^{-/-}Rho^{P23H/P23H}$ mice and are shown relative to levels in age-matched control $ATF6^{+/-}Rho^{+/+}$, $ATF6^{+/-}Rho^{P23H/+}$, and $ATF6^{+/-}Rho^{P23H/P23H}$

Chapter 4 PS19 Mouse Model Exhibits Signs of Retinal Degeneration

4.1 Introduction

The human tau protein is encoded by the microtubule-associated protein tau gene (*MAPT*) and comprises 16 exons on chromosome 17q21 (Andreadis, 2006). Tau is normally distributed into the axons of neurons where it stabilizes microtubules, promotes microtubule assembly, and regulates the dynamic instability of microtubules to allow for cytoskeleton reorganization (Feinstein et al., 2005 and Mandelkow et al., 2012). However, some other functions tau performs are regulating axonal transport through various mechanisms and maintaining the integrity of genomic DNA when it is present in the nucleus (Stamer et al., 2002, Violet et al., 2014 and Sultan et al., 2011).

Under pathological conditions, tau can undergo post-translational modification, such as hyperphosphorylation, acetylation, ubiquitylation, or truncation (Hanger et al., 2009, Min et al., 2010, Shimura et al., 2004 and Corsetti et al., 2015). These post-translational modifications can result in tau detachment from microtubules and, therefore, microtubule disassembly in the axons. Detached tau can have detrimental effects in the neurons. It can mislocalize into presynaptic terminals resulting in synaptic dysfunction, synapse loss, and the reduction in the amount of synaptic vesicles in presynaptic terminals (Decker et al., 2015). Detached tau can also cause similar issues in the dendrites by entering postsynaptic compartments (Hoover et al., 2010). Pathological forms of tau do not have the ability to enter the nucleus, therefore, losing its DNA protective function and resulting in DNA loss (Sultan et al., 2011). Lastly, post-translationally modified tau has the ability to form aggregates that not only leads to dysfunction in the respective neuron its contained in, but these aggregates can be released

into the extracellular space and be taken up by nearby neurons (Zempel et al., 2013 and Wu et al., 2016).

Natively unfolded tau has little tendency to aggregate but under pathological conditions, mutant tau can aggregate into paired helical filaments (PHF) and neurofibrillary tangles (NFT). These aggregates lead to the development of neurodegenerative diseases, otherwise known as tauopathies, such as Alzheimer's disease (AD), progressive supranuclear palsy (PSP), corticobasal degeneration (CBD), and Pick disease (PiD) (Kidd, 1963, Alzheimer, 1907, Lee et al., 2007, and Hutton et al., 1998). The mechanisms in which tau forms aggregates in these neurodegenerative diseases and the pathways involved with tau-induced neurodegeneration are poorly understood but recent studies have helped to contribute to understanding tau pathology. For example, there has been significant evidence highlighting that tau is essential for amyloid-β-induced neurotoxicity and that tau pathology has the ability to spread between neurons (Roberson et al., 2007 and Holmes et al., 2014).

Given that the mechanisms in which tau contributes to the development of tauopathies is poorly understood recent genome-wide association studies (GWAS) were carried out in order to determine common genetic variations that contribute to the risk for development of such brain diseases. GWAS were done on 1,114 individuals with PSP and 3,247 controls followed by a second stage study on 1,051 PSP patients and 3,560 controls revealed previously unidentified single nucleotide polymorphisms (SNPs) associated with PSP risk at *MAPT, STX6, EIF2AK3, and MOBP* (Höglinger et al., 2011). A follow up study of these three SNPs on 796 AD patients and 796 controls further revealed *MOBP* and *EIF2AK3* are associated with APOE ε4-positive patients who have a

Rs242557 SNP at the *MAPT* locus, which is associated with late-onset AD (LOAD) (Liu et al., 2013). Of interest to our lab in these studies is *EIF2AK3*'s association with these two tauopathies given that it is known to code for protein kinase R (PKR)-like endoplasmic reticulum kinase (*PERK*).

Under ER stress conditions, PERK will oligomerize, therefore leading to the activation of its cytosolic kinase domain (Harding et al., 1999). PERK will then phosphorylate eukaryotic translation initiation factor 2 subunit alpha (eIF2α) on the Ser51 residue, which will therefore inhibit translation of new proteins. The phosphorylation of this particular serine residue will inhibit guanine nucleotide exchange factor eIF2B, which is responsible for converting inactive GDP-bound eIF2 to its active GTP-bound form (Harding et al., 1999 and Harding et al., 2002). Through this mechanism, PERK activation helps to alleviate ER stress by decreasing the amount of new polypeptides that require assembly and folding in the ER (Ron et al., 2012). In contrast to this, another consequence of the phosphorylation of eIF2α is the increase in the translation of ATF4, ATF5, and CHOP translational activators (Zhou et al., 2008, Harding et al., 2000 and Palam et al., 2011). ATF4 is known to promote apoptosis through two mechanisms. One mechanism of ATF4 promoted cell death is the transcriptional up-regulation of GADD34, which is responsible for the dephosphorylation of eIF2αP (Novoa et al., 2001). By doing so the initial brake placed on protein synthesis is lifted and protein assembly and folding demands increase in the ER, therefore leading ER stress induced cell death (Han et al., 2013). The second mechanism in which ATF4 promotes cell death is through the transcription of the proapoptic *Chop* gene. CHOP is highly enriched under PERK activation due to both the translational upregulation via eIF2αP and transcriptional

upregulation via ATF4 (Harding et al., 2000, Palam et al., 2011, Lee et al., 2011 and Zinszner et al., 1998). CHOP leads to the upregulation of various apoptotic genes such as *Bim* and *Puma Bcl-2* family genes, *Trb3*, and *Dr5* (Puthalakath et al., 2007, Cazanave et al., 2010, Ohoka et al., 2005 and Yamaguchi et al., 2004).

Given the implications of PERK activation in the tauopathies we aim to answer the question: how does PERK causes neurodegeneration? In order to do so we chose to study these mechanisms *in vivo* with the use of PS19 mice carrying the Endoplasmic Reticulum Stress-Activated Indicator (*ERAI*) gene. The PS19 mouse model is a commonly used to study tauopathies that are associated with the aggregation of tau proteins, resulting in the development of neurofibrillary tangles in the human brain and spinal chord. These mice express a human P301S mutation in the *MAPT* gene driven by the mouse prion protein (*Prnp*) promoter, thereby leading to the expression of the mutant human tau that is fivefold higher than that of endogenous mouse tau protein (Yoshiyama et al, 2007). Tau seeding mainly begins in the hippocampus of the brain and these aggregates have been found to cause further tau aggregation through a prion-like mechanism, causing a spread throughout the rest of the brain and eventually spinal chord (Holmes et al., 2014). Furthermore, since these particular mice used in our studies are the offspring of PS19 mice crossed with mice carrying the *ERAI* gene, they will express the Venus protein when ER stress is present. The Venus protein is a yellow fluorescent GFP variant and will be expressed when the IRE1 pathway of the UPR is activated, which allows for visualization of ER stress in all tissues, including the retina (Iwawaki et al., 2004 and Alavi et al., 2015). This stress indicator gene was constructed by fusing XBP-1 and Venus thereby leading to the translation of the Venus protein under ER stress

conditions (Iwawaki et al., 2004). By using the PS19-ERAI mice we will be able to visual

specifically where ER stress is present in these mice. Given findings that the retina

undergoes pathological changed during the development of AD in humans and there is

tau and phosphorylated tau present in the retinas of PS19 mice, I decided to investigate

whether these mice experience the loss of visual function, retinal degeneration, and ER

stress due to the accumulation of total and phosphorylated tau (Danesh-Meyer et al.,

2006, Paquet et al., 2007, Zhang et al., 2012 and Ho et al., 2012)

4.2 Results

PS19-ERAI mice exhibit retinal degeneration

I performed fundoscopy experiments in order to visualize the entire retina of the wildtype and PS19 mice and found that compared to the wildtype mice, the PS19 mice shows spots of retinal degeneration. This is apparent due to the uneven darker patches that are consistent with patterns seen in eyes of retinitis pigmentosa patients (Figure 9A).

I also performed optical coherence tomography (OCT) images studies and found that there is a significant decrease in the retinal thickness of the PS19 mice in comparison to the wildtype mice (Figure 9B). It is difficult however to distinguish which exactly which layers of the retina is degraded, which would tell me which cell types of the retina are affected in this mouse model.

PS19-ERAI mice exhibit loss of visual function

Through electroretinogram (ERG) studies, I examined the visual function of these PS19-ERAI mice. There are a series of five ERG tests conducted that measure the function of different cell types in the retina. There are three tests done under dark adapated (D.A.) conditions and another two that are done under light adapted (L.A.) conditions. The D.A. scoptopic test measures the function of rod photoreceptor cells based on the amplitude and latency of b-wave of the graph. The D.A. mixed test measures the function of photoreceptors as well as the function of bipolar cells. More specifically, the a-wave measures photoreceptor response and the b-wave measures the function of bipolar cells. The last D.A. test, the oscillatory potential test measures the function of the inner plexiform layer, which houses the retinal ganglion cells. The L.A.

photopic test measures cone function based on the amplitude and latency of the b-wave. The L.A. 10 Hz flicker test measures the post-photoreceptor "on" and "off" pathways, meaning the photoreceptors' ability to recover and response to a new light signal (Frishman, 2013).

In comparison to the wildtype mice, the PS19 mice exhibited a significant decrease in cone and rod photoreceptor function in both eyes as indicated by a much lower amplitude in the b-wave for both scoptopic and photopic tests. The D.A. mixed and oscillatory tests indicate that the left eye (OS) of the PS19 mice experienced more loss of bipolar and retinal ganglion cell function than the right eye (OD) when comparing to the wildtype control. Lastly, the L.A. 10 Hz flicker test revealed that the right eye for the PS19 mice were not able to recover as well to respond to new visual signals compared to the wildtype controls. The left eyes, however, were similar between the two genotypes (Figure 10).

4.3 Discussion

In the initial qualitative studies performed on the PS19-ERAI mice through fundoscopy and OCT techniques show that these mice experience retinal degeneration in comparison to their wildtype counterparts. We can clearly see that there are more dark patches present in the retina of the PS19 mice, indicating retina thinning (Figure 9A). The dark patches are present because a thinner retina allows for the retinal pigment epithelium (RPE) layer to show through. The patchy retina pattern exhibited in the retinas of these mice is consistent with what is seen under RP conditions (Hamel, 2006). Furthermore, when observing the retina thickness of these mice through OCT imaging, it is very apparent that the PS19 retinal layer is much thinning in comparison to the wildtype mice (Figure 9B). As expected, when ERG studies were performed on these animals, it was found that there was a definite decrease in the rod and cone responses of the PS19 mice (Figure 10). There was also a decrease in the function retinal ganglion cells and bipolar cells and the ability of the photoreceptors to turnover to detect new visual signals but the decrease was not as significant as that seen in the rod and cone photoreceptors and the decrease was variable between the left and right eyes (Figure 10).

In all these preliminary studies indicate that there is retinal degeneration and consequent loss of visual function in PS19 mice. However, the mechanism in which this degeneration is caused is still unknown. The next step in these study will be to determine whether the presence of tau and phosphorylated tau is to account for retina dysfunction and whether ER stress, particularly activation of PERK, is present in the retinas of these animals.

4.4 Materials and Methods

Electroretinography

ERG studies were performed on PS19 mice that experienced severe deterioration in their hind leg movement and their littermates, which were all approximately 14-16 months old. Mice were dark-adapted overnight (about 16 hours) before recordings were done. Animals were anesthetized with an intra-peritoneal loading dose of ketamine (93 mg/kg) and xylazine (8 mg/kg). Eyes were treated with 1% topical tropicamide to facilitate pupillary dilation. Each mouse was tested in a fixed state and maneuvered into position for examination within a Ganzfeld bowl (Diagnosys LLC). One active lens electrode was placed on each cornea, with a subcutaneously placed ground needle electrode positioned in the tail and the reference electrodes placed through the lip. Light stimulations were delivered with a xenon lamp at 0.01 and 0.3 cd·s/m^2 in a Ganzfeld bowl. For the photopic ERG measurement, rats were adapted at a background light of 10 cd·s/m^2, and light stimulation was set at 30 cd·s/m^2. The recordings were processed using software supplied by Diagnosys. The a- and b-wave amplitudes were measured from the minimum trough to the maximum peak following light stimulation (Lund et al., 2006, Wang et al., 2010 and Sauvé et al., 2004).

Fundoscopy and Optical Coherence Tomography

In vivo fundus fundoscopy studies was conducted using a SPECTRALIS® high-resolution, spectral domain optical coherence tomography (HRA+OCT) imaging system (Heidelberg Engineering, Inc., Vista, CA, USA). Animals were anesthetized with an intra-peritoneal loading dose of ketamine (93 mg/kg) and xylazine (8 mg/kg). Pupils were dilated with topical 1% atropine and 1% topical tropicamide. PMMA contact lenses

(Cantor & Nissel Ltd) were placed on the eyes prior to imaging to prevent dehydration of the rodent eye and great improve image quality and ease-of-use.
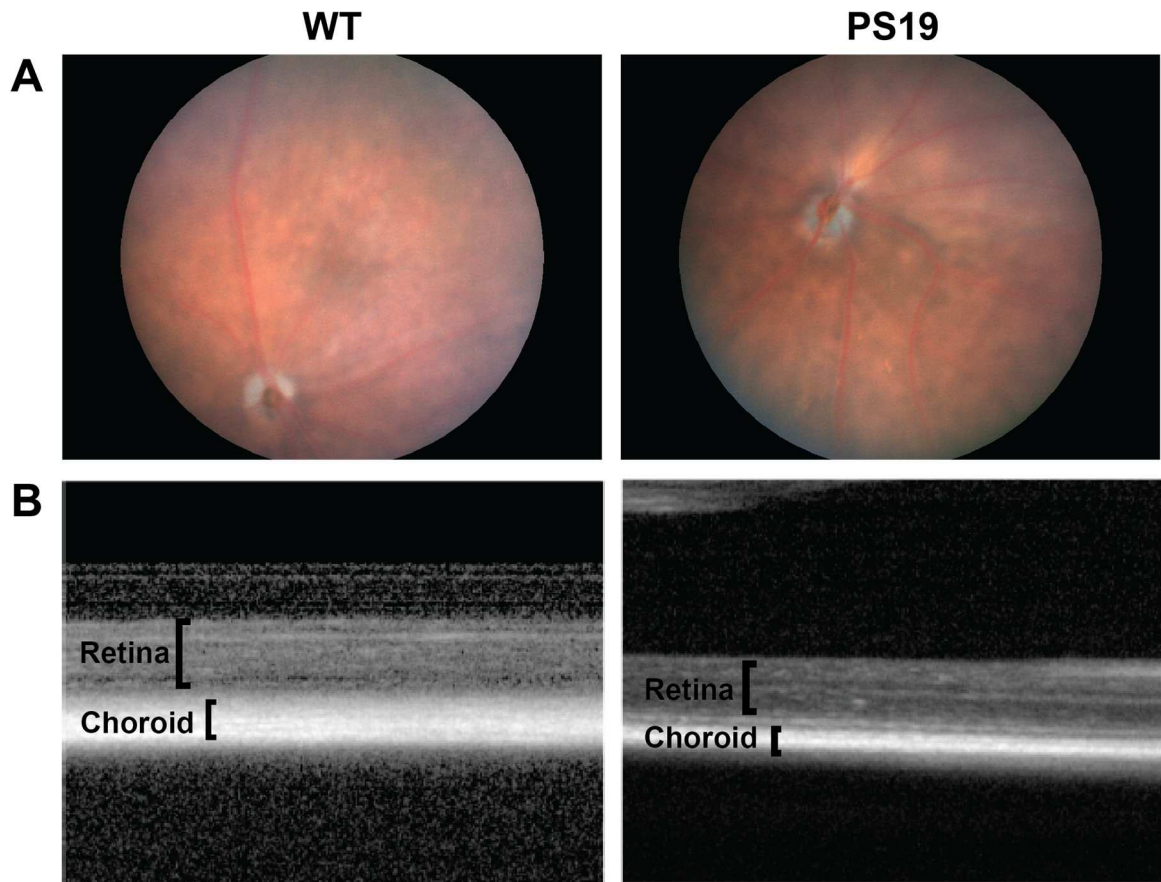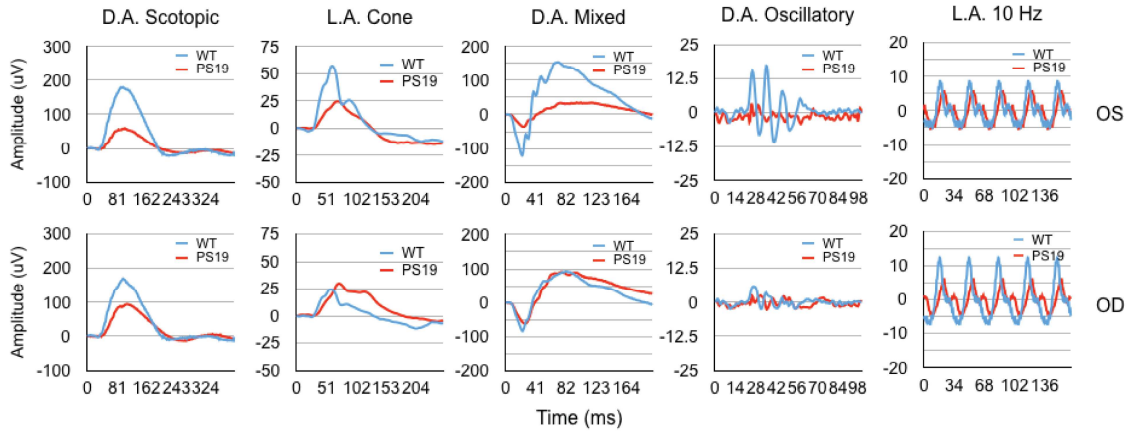
Figure 15. PS19 mice undergo retinal degeneration

Retinal structure of wildtype and PS19 mice. (A) Fundoscopy imaging showed dark patches throughout the image for the PS19 mice compared to littermate wildtype controls, indicating retinal degeneration. (B) OCT analysis showed thinning of the retina in the PS19 mice compared to the wildtype littermate controls.

Figure 16. PS19 mice have decreased visual function

Quantitative evaluation of scotopic, cone, mixed, oscillatory, and 10 Hz flicker data, for wildtype (blue) and PS19 (red) in both the left (OS) and right (OD) eyes. PS19 mice have impaired retinal function compared to wildtype littermates ($n = 4$).

References

M.V. Alavi, W.C. Chiang, H. Kroeger, D. Yasumura, M.T. Matthes, T. Iwawaki, M.M. LaVail, J.H. Lin. In Vivo Visualization of Endoplasmic Reticulum Stress in the Retina Using the ERAI Reporter Mouse. Investigative Opthalmology & Visual Science Invest. Ophthalmol. Vis. Sci. 56 (2015), pp. 6961-6970

B. Alberts. Molecular Biology of the Cell. Garland Science,, New York (2008)

A. Alzheimer. Über eine eigenartige Erkrankung der Hirnrinde. Allg. Z. Psychiatrie Psychisch-gerichtl. Med. 64 (1907), pp. 146–148 (in German)

A. Andreadis. Misregulation of tau alternative splicing in neurodegeneration and dementia. Prog. Mol. Subcell. Biol. 44 (2006), pp. 89–107

M. Ansar, et al. Mutation of ATF6 causes autosomal recessive achromatopsia. Hum. Genet., 134 (2015), pp. 941–950

E.L. Berson. Retinitis pigmentosa. The Friedenwald Lecture. Invest. Ophthalmol. Vis. Sci., 34 (1993), pp. 1659–1676

H. Bommiasamy, S.H. Back, P. Fagone, K. Lee, S. Meschinchi, E. Vink, R. Sriburi, M. Frank, S. Jackowski, R.J. Kaufman, J.W. Brewer. ATF6alpha induces XBP1-independent expansion of the endoplasmic reticulum. J. Cell Sci., 122 (2009), pp. 1626-1636

S.C. Cazanave, N.A. Elmi, Y. Akazawa, S.F. Bronk, J.L. Mott, G.J. Gores. CHOP and AP-1 cooperatively mediate PUMA expression during lipoapoptosis. Am J Physiol Gastrointest Liver Physiol. 299 (2010), pp.G236–G243

B. Chang, T. Grau, S. Dangel, R. Hurd, B. Jurklies, E.C. Sener, S. Andreasson, H. Dolfus, B. Baumann, S. Bolz, N. Artemyev, S. Kohl J. Heckenlively, B. Wissinger. A homologous genetic basis of the murine cpfl1 mutant and human achromatopsia linked to mutations in the PDE6C gene. Proc. Natl. Acad. Sci., 106 (2009), pp. 19581–19586

W.C. Chiang, C. Messah, J.H. Lin. IRE1 directs proteasomal and lysosomal degradation of misfolded rhodopsin. Mol. Biol. Cell, 23 (2012), pp. 758–770

W.C. Chiang, H. Kroeger, S. Sakami, C. Messah, D. Yasumura, M.T. Matthes, J.A. Coppinger, K. Palczewski, M.M. LaVail, J.H. Lin. Robust endoplasmic reticulum-associated degradation of rhodopsin precedes retinal degeneration. Mol. Neurobiol. 52 (2014), pp. 679-695

H.R. Cohen, B. Panning. XIST RNA exhibits nuclear retention and exhibits reduced association with the export factor TAP/NXF1.Chromosoma. (2007); 116 (2007), pp:373-83

V. Corsetti, F. Florenzano, A. Atlante, A. Bobba, M.T. Ciotti, F. Natale, F. Della Valle, A. Borreca, A. Manca, G. Meli, C. Ferraina, M. Feligioni, S. D'Aguanno, R. Bussani, M. Ammassari-Teule, V. Nicolin, P. Calissano, G. Amadoro. NH2-truncated human tau induces deregulated mitophagy in neurons by aberrant recruitment of Parkin and UCHL-1: implications in Alzheimer's disease. Hum. Mol. Genet. 24 (2015), pp. 3058–3081

H.V. Danesh-Meyer. Neuroprotection in glaucoma: recent and future directions. Curr Opin Ophthalmol. 22 (2011), pp. 78–86

J.M. Decker, L. Krüger, A. Sydow, S. Zhao, M. Frotscher, E. Mandelkow, E.M. Mandelkow. Pro-aggregant Tau impairs mossy fiber plasticity due to structural changes and Ca^{++} dysregulation. Acta Neuropathol. Commun. 3(2015), pp. 23

T.P. Dryja, T.L. McGee, E. Reichel, L.B. Hahn, G.S. Cowley, D.W. Yandell, M.A. Sandberg, E.L Berson. A point mutation of the rhodopsin gene in one form of retinitis pigmentosa. Nature, 343 (1990), pp. 364–366

T.P. Dryja, L.B. Hahn, G.S. Cowley, T.L. McGee, E.L. Berson. Mutation spectrum of the rhodopsin gene among patients with autosomal dominant retinitis pigmentosa. Proc. Natl. Acad. Sci. USA, 88 (1991), pp. 9370–9374

T.P. Dryja, T. Li. Molecular genetics of retinitis pigmentosa. Hum. Mol. Genet. (1995), pp. 1739–1743

S.C. Feinstein, L. Wilson. Inability of tau to properly regulate neuronal microtubule dynamics: a loss-of-function mechanism by which tau might mediate neuronal cell death. Biochim. Biophys. Acta 1739 (2005), 268–279 (2005)

M.A. Genead, G.A. Fishman, J. Rha, A.M. Dubis, D.M. Bonci, A. Dubra, E.M. Stone, M. Neitz, J. Caroll. Photoreceptor function in patients with congenital achromatopsia. Invest. Opthalmol. Vis. Sci, 52 (2011), pp. 7298-7308

C. Hetz, B. Mollereau. Disturbance of endoplasmic reticulum proteostasis in neurodegenerative diseases. Nat. Rev. Neurosci., 15 (2014), pp. 233–249

J. Han, S.H. Back, J. Hur, Y.H. Lin, R. Gildersleeve, J. Shan, C.L. Yuan, D. Krokowski, S. Wang, M. Hatzoglou, M.S. Kilberg, M.A. Sartor, R. J. Kaufman. ER-stress-induced transcriptional regulation increases protein synthesis leading to cell death. Nat Cell Biol. 15 (2013), pp. 481–490.

D.P. Hanger, B.H. Anderton, W. Noble. Tau phosphorylation: the therapeutic challenge for neurodegenerative disease. Trends Mol. Med. 15 (2009), pp. 112–119

H.P. Harding, Y. Zhang, D. Ron. Protein translation and folding are coupled by an endoplasmic-reticulum-resident kinase. Nature. 397 (1999), pp. 271–274.

H.P. Harding, I. Novoa, Y. Zhang, H. Zeng, R. Wek, M. Schapira, D. Ron. Regulated translation initiation controls stress-induced gene expression in mammalian cells. Mol Cell. 6 (2000), pp.1099–1108

H.P. Harding, M. Calfon, F. Urano, I. Novoa, D. Ron. Transcriptional and translational control in the Mammalian unfolded protein response. Annu Rev Cell Dev Biol. 18 (2002), pp. 575–599.

K. Haze, H. Yoshida, H. Yanagi, T. Yura, K. Mori. Mammalian transcription factor ATF6 is synthesized as a transmembrane protein and activated by proteolysis in response to endoplasmic reticulum stress. Mol. Biol. Cell, 10 (1999), pp. 3787–3799

N. Hiramatsu, W.C. Chiang, T.D. Kurt, C.J. Sigurdson, J.H. Lin. Multiple mechanisms of unfolded protein response-induced cell death. Am. J. Pathol., 185 (2015), pp. 1800–1808

Y.S. Ho, X. Yang, J.C. Lau, C.H. Hung, S. Wuwongse, Q. Zhang, J. Wang, L. Baum, K.F. So, R.C. Chang. Endoplasmic reticulum stress induces tau pathology and forms a vicious cycle: implication in Alzheimer's disease pathogenesis. J Alzheimers Dis. 28 (2012), pp. 839-854

G.U. Höglinger, N.M. Melhem, D.W. Dickson, P.M. Sleiman, L. Wang, L. Klei, L., G.D. Schellenberg. Identification of common variants influencing risk of the tauopathy progressive supranuclear palsy. Nature Genetics, 43 (2011), pp. 699-705

B.B. Holmes, M.I. Diamond, M. I. Prion-like properties of Tau protein: the importance of extracellular Tau as a therapeutic target. J. Biol. Chem. 289 (2014), pp.19855–19861

B.B. Holmes, J.L. Furman, T.E. Mahan, T.R. Yamasaki, H. Mirbaha, W.C. Eades, L. Belaygorod, N.J. Cairns, D.M. Holtzman, M.I. Diamond. Proteopathic tau seeding predicts tauopathy in vivo. Proc Natl Acad Sci U S A. 111(2014), pp. E4376-4385.

B.R. Hoover, M.N. Reed, J. Su, R.D. Penrod, L.A. Kotilinek, M.K. Grant, R. Pitstick, G.A. Carlson, L.M. Lanier, L.L. Yuan, K.H. Ashe, D. Liao. Tau mislocalization to dendritic spines mediates synaptic dysfunction independently of neurodegeneration. Neuron 68 (2010), pp.1067–1081

M.M. Humphries, D. Rancourt, G.J. Farrar, P. Kenna, M. Hazel, R.A. Bush, P.A. Sieving, D.M. Sheils, P. Creighton, A. Erven, A. Boros, K. Gulya, M.R. Capecchi, P. Humphries. Retinopathy induced in mice by targeted disruption of the rhodopsin gene. Nat. Genet. 15 (1997), pp. 216–219

M. Hutton, C.L. Lendon, P. Rizzu, M. Baker, S. Froelich, H. Houlden, S. Pickering-Brown, S. Chakraverty, A. Isaacs, A. Grover, J. Hackett, J. Adamson, S. Lincoln, D. Dickson, P. Davies, R.C. Petersen, M. Stevens, E. de Graaff, E. Wauters, J. van Baren, M. Hillebrand, M. Joosse, J.M. Kwon, P. Nowotny, L.K. Che, J. Norton[9], J.C. Morris, L.A. Reed, J. Trojanowski, H. Basun, L. Lannfelt, M. Neystat, S. Fahn, F. Dark, T. Tannenberg, P.R. Dodd, N. Hayward, J.B.J. Kwok, P.R. Schofield, A. Andreadis, J. Snowden, D. Craufurd, D. Neary, F. Owen, B.A. Oostra, J. Hardy, A. Goate, J. van Swieten, D. Mann, T. Lynch, P. Heutink. Association of missense and 5′-splice-site mutations in tau with the inherited dementia FTDP-17. Nature 393 (1998), pp. 702–705

M.E. Illing, R.S. Rajan, N.F. Bence, R.R. Kopito. A rhodopsin mutant linked to autosomal dominant retinitis pigmentosa is prone to aggregate and interacts with the ubiquitin proteasome system. J. Biol. Chem., 277 (2002), pp. 34150–34160

T. Iwawaki, R. Akai, K. Kohno, M. Miura M. A transgenic mouse model for monitoring endoplasmic reticulum stress. Nat Med. 10 (2004), pp. 98–102.

S. Kaushal, H.G. Khorana. Structure and function in rhodopsin. 7. Point mutations associated with autosomal dominant retinitis pigmentosa. Biochemistry, 33 (1994), pp. 6121–6128

M. Kidd. Paired helical filaments in electron microscopy of Alzheimer's disease. Nature 197(1963), pp. 192–193

S. Kohl, T. Marx, L. Giddings, H. Jägle, S.G. Jacobson, E. Apfelstedt-Sylla, E. Zrenner, L.T. Sharpe, B. Wissinger. Total colourblindness is caused by mutations in the gene encoding the alpha-subunit of the cone photoreceptor cGMP-gated cation channel. Nat. Genet., 19 (1998), pp. 257–259

S. Kohl, B. Baumann, M. Broghammer, H. Jägle, P. Siieving, U. Sellner, R. Spegal, M. Anastasi, E. Zrenner, L.T. Sharpe, B. Wissinger. Mutations in the CNGB3 gene encoding the beta-subunit of the cone photoreceptor cGMP-gated channel are responsible for achromatopsia (ACHM3) linked to chromosome 8q21. Hum. Mol. Genet., 9 (2000), pp. 2107–2116

S. Kohl, F. Coppieters, F. Meire, S. Schaich, S. Roosing, C. Brennenstuhl, S. Bolz, M.M. van Genderen, F.C. Riemslag, the European Retinal Disease Consortium, R. Lukowski, A.I. den Hollander, F.P. Cremers, E. De Baere, C.B. Hoyng, B.

Wissinger. A nonsense mutation in PDE6H causes autosomal-recessive incomplete achromatopsia. Am. J. Hum. Genet., 91 (2012), pp. 527–532

S. Kohl, D. Zobor, W.C. Chiang, N. Weisschuh, J. Staller, I. Gonzalez Menendez, S. Chang, S.C Beck, M. Garcia Garrido, V. Sothilingam, M.W. Seeliger, F. Stanzia, F. Benedicenti, F. Inzana, E. Héon, A. Vincent, J. Beis, T.M. Strom, G. Rudolph, S. Roosing, A. I den Hollander, F.P.M Cremers, I. Lopez, H. Ren, A.T. Moore, A.R. Webster, M. Michaelides, R.K. Koenekoop, E. Zrenner, R.J. Kaufman, S.H. Tsang, B. Wissinger, J.H. Lin. Mutations in the unfolded protein response regulator ATF6 cause the cone dysfunction disorder achromatopsia. Nat. Genet. (2015)

H. Kroeger, M.M. LaVail, J.H. Lin. Endoplasmic reticulum stress in vertebrate mutant rhodopsin models of retinal degeneration. Adv. Exp. Med. Biol., 801 (2014), pp. 585–592

A.H. Lee, N.N. Iwakoshi, L.H. Glimcher. XBP-1 regulates a subset of endoplasmic reticulum resident chaperone genes in the unfolded protein response. Mol. Cell. Biol., 23 (2003), pp. 7448–7459

H.C. Lee, Y.J. Chen, Y.W. Liu, K.Y. Lin, S.W. Chen, C.Y. Lin, Y.C. Lu, P.C. Hsu, S.C. Lee, H.J. Tsai. Transgenic zebrafish model to study translational control mediated by upstream open reading frame of human chop gene. Nucleic Acids Res. 39 (2011) pp. e139.

V.M. Lee, M. Goedert, J.Q. Trojanowski. Neurodegenerative tauopathies. Annu. Rev. Neurosci. 24 (2001), pp.1121–1159

J.H. Lin, H. Li, D. Yasumura, H.R. Cohen, C. Zhang, B. Panning, K.M. Shokat, M.M. Lavail, P. Walter. IRE1 signaling affects cell fate during the unfolded protein response. Science, 318 (2007), pp. 944–949

Q. Liu, J. Yu, D. Miao, X. Ma, H. Wang, W. Wang, L. Tan. (2013). An exploratory study on STX6, MOBP, MAPT, and EIF2AK3 and late-onset Alzheimer's disease. Neurobiology of Aging, 34 2013), pp. 1519

E.M. Mandelkow, E. Mandelkow. Biochemistry and cell biology of tau protein in neurofibrillary degeneration. Cold Spring Harb. Perspect. Med. 2 (2012), a006247

S.W. Min, S.H. Cho, Y. Zhou, S. Schroeder, V. Haroutunian, W.W. Seeley, E.J. Huang, Y. Shen, E. Masliah, C. Mukherjee, D. Meyers, P.A. Cole, M. Ott, L. Gan. Acetylation of tau inhibits its degradation and contributes to tauopathy. Neuron 67 (2010), 953–966

S. Nadanaka, H. Yoshida, F. Kano, M. Murata, K. Mori. Activation of mammalian unfolded protein response is compatible with the quality control system operating in the endoplasmic reticulum. Mol. Biol. Cell. 15 (2004), pp. 2537-2548

I. Novoa, H. Zeng, H.P. Harding, D. Ron. Feedback inhibition of the unfolded protein response by GADD34-mediated dephosphorylation of eIF2alpha. J Cell Biol. 153 (2001), pp. 1011–1022.

N. Ohoka, S. Yoshii, T. Hattori, K. Onozaki, H. Hayashi. TRB3, a novel ER stress-inducible gene, is induced via ATF4-CHOP pathway and is involved in cell death. EMBO J. 24 (2005), pp.1243–1255

L.R. Palam, T.D. Baird, R.C. Wek. Phosphorylation of eIF2 facilitates ribosomal bypass of an inhibitory upstream ORF to enhance CHOP translation. J Biol Chem. 286 (2011), pp. 10939–10949.

K. Palczewski. G protein-coupled receptor rhodopsin. Annu. Rev. Biochem., 75 (2006), pp. 743–767

K. Palczewski. Chemistry and biology of vision. J. Biol. Chem., 287 (2012), pp. 1612–1619

F.R. Papa. Bypassing a Kinase Activity with an ATP-Competitive Drug. Science, 302 (2003), pp: 1533-1537

C. Paquet, M. Boissonnot, F. Roger, P. Dighiero, R. Gil, J. Hugon. Abnormal retinal thickness in patients with mild cognitive impairment and Alzheimer's disease. Neuroscience Letters, 420 (2007), pp. 97-99

C.M. Pickart.Mechanisms Underlying Ubiquitination. Annu. Rev. Biochem. Annual Review of Biochemistry, 70 (2001), pp. 503-533

H. Puthalakath, L.A. O'Reilly, P. Gunn, L. Lee, P.N. Kelly, N.D. Huntington, P.D. Hughes, E.M. Michalak, J. McKimm-Breschkin, N. Motoyama, T. Gotoh, S. Akira, P. Bouillet, A. Strasser. ER stress triggers apoptosis by activating BH3-only protein Bim. Cell. 129 (2007), pp. 1337–1349

E.D. Roberson, E.D. Roberson, K. Scearce-Levie, J.J. Palop, F. Yan, I.H. Cheng, T. Wu, H. Gerstein, G.Q. Yu, L. Mucke. Reducing endogenous tau ameliorates amyloid β-induced deficits in an Alzheimer's disease mouse model. Science 316 (2007), pp. 750–754

D. Ron, H.PP. Harding. Protein-folding homeostasis in the endoplasmic reticulum and nutritional regulation. Cold Spring Harb Perspect Biol. 4 (2012), pii: a013177

D.T. Rutkowski, . Adaptation to ER stress is mediated by differential stabilities of pro-survival and pro-apoptotic mRNAs and proteins. PLos Biol., 4 (2006), e374

S. Sakami, T. Maeda, G. Bereta, K. Okano, M. Golczak, A. Sumaroka, A.J. Roman, A.V. Cideciyan, S.G. Jacobson, K. Palczewski. Probing mechanisms of photoreceptor degeneration in a new mouse model of the common form of autosomal dominant retinitis pigmentosa due to P23H opsin mutations. J. Biol. Chem., 286 (2011), pp. 10551–10567

R.S. Saliba, P.M. Munro, P.J. Luthert, M.E. Cheetham. The cellular fate of mutant rhodopsin: quality control, degradation and aggresome formation. J. Cell Sci., 115 (2002), pp. 2907–2918

J. Shen, X. Chen, L. Hendershot, R. Prywes. ER stress regulation of ATF6 localization by dissociation of BiP/GRP78 binding and unmasking of Golgi localization signals. Dev Cell, 3 (2002), pp. 99-111

H. Shimura, D. Schwartz, S.P. Gygi, K.S. Kosik. CHIP–Hsc70 complex ubiquitinates phosphorylated tau and enhances cell survival. J. Biol. Chem. 279 (2004), 4869–4876

M.D. Shoulders, L.M. Ryno, J.C. Genereux, J.J. Moresco, P.G. Tu, C. Wu, J.R. Yates III, A.I. Su, J.W. Kelly, R.L. Wiseman. Stress-independent activation of XBP1s and/or ATF6 reveals three functionally diverse ER proteostasis environments. Cell Rep., 3 (2013), pp. 1279–1292

K. Stamer, R. Vogel, E. Thies, E. Mandelkow, E.M. Mandelkow. Tau blocks traffic of organelles, neurofilaments, and APP vesicles in neurons and enhances oxidative stress. J. Cell Biol. 156 (2002), pp. 1051–1063

A. Sultan, F. Nesslany, M. Violet, S. verine Be´gard, A. Loyens, S. Talahari, Z. Mansuroglu, D. Marzin, N. Sergeant, S. Humez, M. Colin, E. Bonnefoy, L. Bue´ e, M.C. Galas. Nuclear tau, a key player in neuronal DNA protection. J. Biol. Chem. 286 (2011), pp. 4566–4575

C.H. Sung, B.G. Schneider, N. Agarwal, D.S. Papermaster, J. Nathans. Functional heterogeneity of mutant rhodopsins responsible for autosomal dominant retinitis pigmentosa. Proc. Natl. Acad. Sci. USA, 88 (1991), pp. 8840–8844

C.H. Sung, J.Z. Chuang. The cell biology of vision. J. Cell Biol., 190 (2010), pp. 953–963

I. Tabas, D. Ron. Integrating the mechanisms of apoptosis induced by endoplasmic reticulum stress. Nature Cell Biology, 13(2011), pp.184-190

A.A. Thiadens, A.I. den Hollander, S. Roosing, S.B. Nabuurs, R.C. Zekveld-Vroon, R.W.J. Collin, E. De Baere, R.K. Koenekoop, M.J. van Schooneveld, T.M. Strom, J.J.C. van Lith-Verhoeven, A.J. Lotery, N. van Moll-Ramirez, B.P. Leroy, L.I. van den Born, C.B. Hoyng, F.P.M. Cremers, C.C.W. Klaver. Homozygosity mapping reveals PDE6C mutations in patients with early-onset cone photoreceptor disorders. Am. J. Hum. Genet., 85 (2009), pp. 240–247

W. Tirasophon, K. Lee, B. Callaghan, A. Welihinda, R.J. Kaufman. The endoribonuclease activity of mammalian IRE1 autoregulates its mRNA and is required for the unfolded protein response. Genes Dev 14 (2000), pp: 2725-36

M. Violet, L. Delattre, M. Tardivel, A. Sultan, A. Chauderlier, R. Caillierez, S. Talahari, F. Nesslany, B. Lefebvre, E. Bonnefoy, L. Buée, M.C. Galas. A major role for Tau in neuronal DNA and RNA protection in vivo under physiological and hyperthermic conditions. Front. Cell Neurosci. 8 (2014), pp. 84

P. Walter, D. Ron. The unfolded protein response: from stress pathway to homeostatic regulation. Science, 334 (2011), pp. 1081–1086

M. Wang, R.J. Kaufman. Protein misfolding in the endoplasmic reticulum as a conduit to human disease. Nature, 529 (2016), pp. 326–335

X. Z. Wang, H.P. Harding, Y. Zhang, E.M. Jolicoeur, M. Kuroad, D. Ron. Cloning of mammalian Ire1 reveals diversity in the ER stress responses. The EMBO Journal, 19 (1998), pp: 5708-5717

B.S. Winkler BS The electroretinogram of the isolated rat retina. Vision Res. 12 (1972), pp. 1183–1198.

M.T. Wong-Riley. Energy metabolism of the visual system. Eye Brain, 2 (2010), pp. 99–116

J. Wu, D.T. Rutkowski, M. Dubois, J. Swathirajan, T. Saunders, J. Wang, B. Song, R.J. Kaufman. ATF6alpha optimizes long-term endoplasmic reticulum function to protect cells from chronic stress. Dev. Cell, 13 (2007), pp. 351–364

J.W. Wu, S.S. Hussaini, I.M. Bastille, G.A. Rodriguez, A. Mrejeru, L. Rilett, D.W. Sanders, C. Cook, H. Fu, R.A. Boonen, M. Herman, E. Nahmani, S. Emrani, Y.H. Figueroa, M.I. Diamond, C.L. Clelland, S. Wray, K.E. Duff. Neuronal activity enhances tau propagation and tau pathology in vivo. Nat Neurosci. 19 (2016), pp. 1085-1092

M. Xu, V. Gelowani, A. Eblimit, F. Wang, M.P. Young, B.L. Sawyer, L. Zhao, G. Jenkins, D.J. Creel, K. Wang, Z. Ge, H. Wang, Y. Li, M.E. Hartnett, R. Chen.

ATF6 is mutated in early onset photoreceptor degeneration with macular involvement. Invest. Ophthalmol. Vis. Sci., 56 (2015), pp. 3889–3895

H. Yamaguchi, H.G. Wang. CHOP is involved in endoplasmic reticulum stress-induced apoptosis by enhancing DR5 expression in human carcinoma cells. J Biol Chem. 279 (2004), pp. 45495–45502

K. Yamamoto, T. Sato, T. Matsui, M. Sato, T. Okada, H. Yoshida, A. Harada, K. Mori. Transcriptional induction of mammalian ER quality control proteins is mediated by single or combined action of ATF6alpha and XBP1. Dev. Cell, 13 (2007), pp. 365–376

L.P. Yang, L.M. Wu, X.J. Guo, Y. Li, M.O. Tso. Endoplasmic reticulum stress is activated in light-induced retinal degeneration. Journal of neuroscience research. 86 (2008), pp.910-919

J. Ye, R.B. Rawson, R. Komuro, X. Chen, U.P. Davé, R. Prywes, M.S. Brown, J.L. Goldstein. ER stress induces cleavage of membrane-bound ATF6 by the same proteases that process SREBPs. Mol. Cell, 6 (2000), pp. 1355–1364

Y. Yoshiyama, M. Higuchi, B. Zhang, S.M. Huang, N. Iwata, T.C. Saido, J. Maeda, T. Suhara, J.Q. Trojanowski, V.M. Lee. Synapse loss and microglial activation precede tangles in a P301S tauopathy mouse model. Neuron. 53 (2007), pp.337-351

H. Zempel, J. Luedtke, Y. Kumar, J. Biernat, H. Dawson, E. Mandelkow, E.M. Mandelkow. Amyloid-β oligomers induce synaptic damage via Tau-dependent microtubule severing by TTLL6 and spastin. EMBO J. 32 (2013), 2920–2937

A.B. Zetoune, S. Fontanière, D. Magnin, O. Anczuków, M. Buisson, C.X. Zhang, S. Mazoyer. Comparison of nonsense-mediated mRNA decay efficiency in various murine tissues. *BMC Genet BMC Genetics, 9* (2008), pp. 83

B. Zhang, J. Carroll, Q. Trojanowski, Y. Yao, M. Iba, J.S. Potuzak, K.R. Brunden. The Microtubule-Stabilizing Agent, Epothilone D, Reduces Axonal Dysfunction, Neurotoxicity, Cognitive Deficits, and Alzheimer-Like Pathology in an Interventional Study with Aged Tau Transgenic Mice. Journal of Neuroscience, 32 (2012), pp. 3601-3611

S.X. Zhang, J.H. Ma, M. Bhatta, S.J. Fliesler, J.J. Wang. The unfolded protein response in retinal vascular diseases: implications and therapeutic potential beyond protein folding. Prog. Retin. Eye Res., 45 (2015), pp. 111-131

S.X. Zhang, E. Sanders, S.J. Fliesler, J.J. Wang. Endoplasmic reticulum stress and the folded protein responses in retinal degeneration. Experimental Eye Research. 125 (2014), pp. 30-40

D. Zhou, L.R. Palam, L. Jiang, J. Narasimhan, K.A. Staschke, R.C. Wek. Phosphorylation of eIF2 directs ATF5 translational control in response to diverse stress conditions. J Biol Chem. 283 (2008), pp.7064–7073.

H. Zinszner, M. Kuroda, X. Wang, N. Batchvarova, R.T. Lightfoot, H. Remotti, J.L. Stevens, D. Ron. CHOP is implicated in programmed cell death in response to impaired function of the endoplasmic reticulum. Genes Dev. 12 (1998), pp.982–995.